Small-molecule Activation of TFEB Alleviates Niemann-Pick Disease Type C via Promoting Lysosomal Exocytosis and Biogenesis

Kaili Du[1,2,3], Hongyu Chen[1,3], Zhaonan Pan[1], Mengli Zhao[1],
Shixue Cheng[1], Yu Luo[1], Wenhe Zhang[1], Dan Li[1,2,#]

[1]Collaborative Innovation Center of Yangtze River Delta Region Green Pharmaceuticals, College of Pharmaceutical Sciences, Zhejiang University of Technology, Hangzhou 310014, China

[2]Department of Molecular, Cellular, and Developmental Biology, University of Michigan, 3089 Natural Science Building (Kraus), 830 North University Avenue, Ann Arbor, MI 48109, USA

Running Title: *Induction of Lysosomal Exocytosis and Biogenesis via TFEB activation for the treatment of Niemann-Pick Disease Type C*

Key words: *TFEB agonists; Cholesterol accumulation; NPC1; Lysosome*

[3]These authors contributed equally

Correspondence should be addressed to: D. L. (Email: **lidan@zjut.edu.cn**)

Abstract

Niemann–Pick disease type C (NPC) is a devastating lysosomal storage disease characterized by abnormal cholesterol accumulation in lysosomes. Currently, there is no treatment for NPC. Transcription factor EB (TFEB), a member of the microphthalmia transcription factors (MiTF), has emerged as a master regulator of lysosomal function and promoted the clearance of substrates stored in cells. However, it is not known whether TFEB plays a role in cholesterol clearance in NPC disease. Here, we show that transgenic overexpression of TFEB, but not TFE3 (another member of MiTF family) facilitates cholesterol clearance in various NPC1 cell models. Pharmacological activation of TFEB by sulforaphane (SFN), a previously identified natural small-molecule TFEB agonist by us, can dramatically ameliorate cholesterol accumulation in human and mouse NPC1 cell models. In NPC1 cells, SFN induces TFEB nuclear translocation via a ROS-Ca^{2+}-calcineurin dependent but MTOR-independent pathway and upregulates the expression of TFEB-downstream genes, promoting lysosomal exocytosis and biogenesis. While genetic inhibition of TFEB abolishes the cholesterol clearance and exocytosis effect by SFN. In the NPC1 mouse model, SFN dephosphorylates/activates TFEB in brain and exhibits potent efficacy of rescuing the loss of Purkinje cells and body weight. Hence, pharmacological upregulating lysosome machinery via targeting TFEB represents a promising approach to treat NPC and related lysosomal storage diseases, and provides the possibility of TFEB agonists ie SFN as potential NPC therapeutic candidates.

Abbreviation: ACP, acid phosphatase; AREs, antioxidant response elements; ANOVA, analyses of variance; BBB, blood–brain barrier; BSA, bovine serum albumin; CLEAR, coordinated lysosomal expression and regulation; CsA, cyclosporin A; FBS, fetal bovine serum; KD, knockdown; KO, knockout; LAMP1, lysosomal associated membrane protein 1; ROS: reactive oxygen species; LSDs, lysosomal storage diseases; MEF, mouse embryonic fibroblast; MiTF, microphthalmia/TFE transcriptional factor; MTOR, mechanistic target of rapamycin kinase complex 1; NAC: N-acetylcysteine; NAGase, β- hexosaminidase; NPC, Niemann-Pick type C disease; OE, overexpression;

PM, plasma membrane; RPS6 KB1/ p70S6K, ribosomal protein S6 kinase B1; SFN, sulforaphane; TFEB, transcription factor EB.

Introduction

Lysosomes are essential organelles for the degradation and recycle of damaged complex substrates and organelles (Xu and Ren 2015). In recent years, lysosomes have emerging roles in plasma membrane repair, external environmental sensing, autophagic cargo sensing, and proinflammatory response, thereby regulating fundamental processes such as cellular clearance and autophagy (Tsunemi, Perez-Rosello et al. 2019). Mutations in genes encoding lysosomal proteins could result in more than approximately 70 different lysosomal storage disorders (Fraldi, Klein et al. 2016). Niemann-Pick disease type C (NPC) is a rare lysosomal storage disorder caused by mutation in either *NPC1* or *NPC2* gene. Deficiency in NPC1 or NPC2 protein results in late endosomal/lysosomal accumulation of unesterified cholesterol (Sarkar, Carroll et al. 2013, Spampanato, Feeney et al. 2013). Clinical symptoms of NPC include hepatosplenomegaly, progressive neurodegeneration and central neurol system dysfunction ie. seizure, motor impairment, and decline of intellectual function (Carstea, Morris et al. 1997). So far there is no FDA-approved specific therapy for NPC, although miglustat, approved to treat type I Gaucher disease, has been used for NPC treatment in countries including China, Canada and European Union (Pineda, Wraith et al. 2009, Pineda, Perez-Poyato et al. 2010, Wraith, Vecchio et al. 2010, Chien, Peng et al. 2013)

Transcription factor EB (TFEB), a member of the microphthalmia/TFE transcription factor (MiTF) family, is identified as a master regulator of lysosome and autophagy by controlling the “coordinated lysosomal expression and regulation” (CLEAR) network, covering genes associated to lysosomal exocytosis and biogenesis, and autophagy (Sardiello and Ballabio 2009, Martini-Stoica, Xu et al. 2016, Napolitano and Ballabio 2016). In normal condition, TFEB is phosphorylated by mTOR kinase and kept in cytosol inactively (Martina and Rosa 2018, Napolitano, Esposito et al. 2018). Under stress conditions ie. starvation or oxidative stress, TFEB is dephosphorylated and actively translocates into nucleus, promoting the expression of genes associated with lysosome and autophagy (Medina, Diego et al. , Zhang, Cheng et al. 2016, Puertollano, Ferguson et al. 2018). TFEB overexpression or activation results in increased number of lysosomes, autophagy flux and exocytosis (Medina, Fraldi et al. 2011, Settembre, Di Malta et al. 2011, Giatromanolaki, Kalamida et al. 2015, Xu, Du et al. 2020), which may trigger cellular clearance. In fact, it is

reported that TFEB overexpression promotes cellular clearance and ameliorates the phenotypes in a variety of neurodegenerative diseases including Alzheimer's, Parkinson's, and Huntington's. (Sardiello, Palmieri et al. 2009, Tsunemi and La Spada 2012, Decressac and Björklund 2013, Polito, Li et al. 2014, Ballabio 2016, Napolitano and Ballabio 2016). Moreover, upregulation of TFEB has been reported to benefit lysosomal storage diseases (LSDs), such as Pompe disease (Argüello, Balboa et al. 2021). However, it is not known whether upregulation of TFEB by genetic or pharmacological methods is sufficient to increase lysosomal function and alleviate NPC phenotypes *in vitro* or *in vivo*. If so, TFEB may be a putative target for NPC treatment and manipulating lysosomal function via small-molecule TFEB agonists may have broad therapeutic potential for NPC.

Results

Transgenic overexpression or pharmacological activation of TFEB reduces cholesterol accumulation in various human NPC1 cell models

TFEB and TFE3 are identified as key transcription factors regulating lysosome and autophagy biogenesis (Sardiello, Palmieri et al. 2009). To investigate the role of TFEB/TFE3 in cellular cholesterol levels in NPC1 cells, HeLa cells were treated with U18666A (2.5 μM, an inhibitor of the endosomal/lysosomal cholesterol transporter NPC1), a drug that has been widely used to induce NPC phenotype in cell models (Poh, Shui et al. 2012) (Thereafter HeLa NPC1 cells represent U18666A-treated HeLa cells). Cellular cholesterol levels were measured by the well-known cholesterol-marker filipin (Lu, Liang et al. 2015). As shown in **Fig. 1A, B**, in HeLa NPC1 cells overexpressing TFEB-mCherry or TFEB^{S211A}-mCherry (S211 non-phosphorylatable mutant, a constitutively active TFEB) (Wang, Gao et al. 2015), the cellular cholesterol levels (filipin) were significantly diminished compared to non-expressed or mCherry-only transfected NPC1 cells. In contrast, TFE3-GFP overexpression displayed no obvious reduction of cholesterol levels in HeLa NPC1 cells (***Fig. S1A, B***). Hence, TFEB but not TFE3 contributes to cholesterol reduction in NPC1 cells.

Pharmacological activation of TFEB is an emerging strategy for LSD treatment (Levine and Kroemer 2008). We have previously identified a natural TFEB agonist-sulforaphane (SFN), which is also an activator of cellular antioxidant NFE2L2/Nrf2 pathway,

dramatically mitigating oxidative stress commonly associated with metabolic and age-related diseases including NPC diseases (Corssac, Campos-Carraro et al. 2018, Li, Shao et al. 2021, Liu, Fu et al. 2021). Based on our previous data that SFN (10-15 μM, 3–24 h) potently activates TFEB in various cell lines, promoting lysosomal function (Li, Shao et al. 2021), thus, in this study, we set SFN treatment dose to 15 μM and treatment time to 4-24 h according to individual experiment. We hypothesize that SFN may contribute to cholesterol clearance in NPC disease. To evaluate this hypothesis, we first examined the effect of SFN on cellular cholesterol levels in HeLa NPC1 cell model using filipin staining. As shown in **Fig. 1C, D**, U18666A treatment significantly increased filipin signals in bright perinuclear granules, which were well co-localized with lysosomal marker LAMP1, but not with ER marker calnexin in HeLa cells (***Fig. S2A, B***), suggesting that U18666A-isnduced cholesterol accumulation presents in the late endosome/lysosome compartment, but not in ER. Moreover, when HeLa NPC1 cells were further challenged with SFN (15 μM, 12-24 h), a dramatically reduction of cholesterol accumulation (filipin intensity) by more than 30% was observed in lysosomes (**Fig. 1C-E, *Fig. S2C, D***). These results confirmed that U18666A interferes with the egress of free cholesterol from endosomes/lysosomes as previously reported by others (Lange and Steck 1994, Davis, Shin et al. 2021) and SFN reduces lysosomal cholesterol in NPC1 cells.

In our previous study, we identified that SFN activates TFEB via a ROS-Ca^{2+}-calcineurin-mediated but MTOR (mechanistic target of rapamycin kinase)-independent mechanism (Li, Shao et al. 2021). Thus, we further validated this mechanism of SFN in HeLa NPC1 cell model by performing immunofluorescence experiments. In HeLa NPC1 cells, SFN (15 μM, 24 h) induced robust TFEB translocation from the cytosol to the nucleus (**Fig. 1F, G**). SFN treatment (15 μM, 24 h) also resulted an increase in the mRNA levels of TFEB downstream genes, including genes required for autophagy (*ULK1*, *SQSTM1* and *ATG5*) and lysosome biogenesis-*LAMP1*, using quantitative real-time PCR (Q-PCR) (**Fig. 1H)**. Consistent with previous finding, BAPTA-AM (a membrane-permeable Ca^{2+} chelator), FK506 and cyclosporin A (CsA) (calcineurin inhibitors) and N-acetylcysteine (NAC, a ROS scavenger) can robustly block SFN-induced TFEB nuclear translocation in HeLa NPC1 cells (***Fig. S3)***, suggesting that in NPC1 cells SFN induces TFEB nuclear translocation via a ROS-

Ca^{2+}-calcineurin dependent mechanism A key mechanism of TFEB activation is Ca^{2+}-dependent dephosphorylation of TFEB by protein phosphatases (Medina, Diego et al. , Martina and Puertollano 2018). We next investigated the specific phosphorylated site on TFEB by SFN in NPC1 cells. Following 24 h exposure to SFN, S211 and S142-TFEB phosphorylation were significantly decreased (**Fig. 1I, J)**, while S122 phosphorylation was not affected. These results indicate that TFEB is dephosphorylated at S211 and S142 residues by SFN in HeLa NPC1 model. TFEB nuclear shuffling is regulated by the activity of MTOR, which is regulated by its phosphorylation status (Martina, Chen et al. 2012). SFN reportedly activates TFEB in a mTOR-independent manner (Li, Shao et al. 2021). Consistently, no significant inhibition of phosphorylated MTOR (p-MTOR) or RPS6KB1 (p-RPS6KB1) can be observed in HeLa NPC1 cells treated with SFN (15 μM, 24 h) (***Fig. S4A, B***). Therefore, in HeLa NPC1 cells SFN-induced TFEB activation is unlikely to be mediated by MTOR inhibition. We also examined the possibility of the direct effect of SFN on NPC1 by western blotting. As shown in ***Fig. S5***, SFN (15 μM, 24 h) treatment did not affect NPC1 expression in human NPC1-patient fibroblasts. Give the well-known role of SFN as a NFE2/Nrf2 inducer, we also validated whether SFN can induce Nrf2 activation in NPC cells. As shown in ***Fig. S6A, B***, SFN (15 μM, 24 h) induced robust Nrf2 nuclear translocation from the cytosol to the nucleus in HeLa NPC1 and NPC primary mouse embryonic fibroblasts (MEF) cells.

Next, we verified the effect of SFN in another NPC1 cell model by knockdown (KD) *NPC1* with specific siRNA (Liao, Wang et al. 2015, Hoglinger, Burgoyne et al. 2019). In *NPC1* KD HeLa cells with more than 80 % knockdown efficiency (**Fig. 2A**), SFN can induce TFEB nuclear translocation (**Fig. 2B, C**) and upregulate its downstream gene expression (**Fig. 2D**). Notably, SFN (15 μM, 24 h) treatment significantly reduced cholesterol levels in *NPC1* KD cells (**Fig. 2E, F)**. Similar results were observed in human NPC1-patient fibroblast cells. SFN treatment robustly promoted TFEB nuclear translocation (**Fig. 2G, H**) and cholesterol clearance (**Fig. 2I, J**). Taken together, these experiments demonstrate that pharmacological activation of TFEB activation by SFN could promote cellular cholesterol clearance in various NPC *in vitro* models.

TFEB is required in SFN -promoted cholesterol clearance in NPC1 cells

We next investigated whether TFEB is required for SFN-promoted cholesterol clearance using two strategies. On one hand, HeLa cells were treated with the siRNAs specifically against TFEB or transiently overexpressed with mCherry-TFEB. The efficiency of siRNA KD and overexpression was evaluated by western blot (**Fig. 3A**). In the si*TFEB*-transfected HeLa NPC1 cells, SFN-promoted (15 μM, 24 h) cholesterol clearance was almost abolished (**Fig. 3B, C**). In contrast, in scrambled siRNA-transfected NPC1 cells, the cholesterol levels were significantly reduced by more than 30% by SFN. Notably, TFEB overexpression-induced reduction of cholesterol can be further boosted about 20% by SFN treatment (**Fig. 3B, C**). On the other hand, HeLa *TFEB* KO cells was constructed by the CRISPR/Cas9 tool (**Fig. 3D**). Consistently, SFN failed to diminish cholesterol in HeLa *TFEB* KO cells, whereas re-expression of a recombinant TFEB restored the cholesterol clearance by SFN (**Fig. 3E, F**). Collectively, these data indicate that TFEB is specifically required for lysosomal cholesterol reduction upon SFN treatment.

SFN promotes lysosomal exocytosis and biogenesis in human NPC1 models in a TFEB-dependent manner

We then studied the mechanism by which SFN led to diminish cellular cholesterol in NPC1 cells. Considering the established role of TFEB activation in lysosomal exocytosis, we verified the hypothesis that SFN-induced cholesterol clearance through upregulation of lysosomal exocytosis using surface LAMP1 immunostaining (**Fig. 4A**). When lysosomal exocytosis processes, luminal lysosomal membrane proteins can be detected on the extracellular side of the plasma membrane (PM) by measuring surface expression of LAMP1 (lysosomal associated membrane protein 1), a resident marker protein of late endosomes and lysosomes (referred to as “lysosomes” for simplicity hereafter) with a monoclonal antibody against a luminal epitope of LAMP1 (Reddy, Caler et al. 2001). After incubation with SFN (15 μM) for 24 h, HeLa NPC1 cells exhibited a dramatic increase in the signal of LAMP1 staining in the PM (Surface LAMP1 signal colocalized with DiO, a PM marker) compared to untreated control cells (**Fig. 4A, B**), suggesting an increase of lysosomal exocytic process. Likewise, SFN promoted lysosomal exocytosis in primary macrophage cells (***Fig. S7A***). In

contrast, this increase of surface LAMP1 signal by SFN was significantly reduced in *TFEB* KO cells (***Fig. S7B***), demonstrating that SFN-induced lysosomal exocytosis is TFEB-dependent.

A direct consequence of lysosomal exocytosis is the release of lysosomal contents into the cell culture medium (Rodriguez, Webster et al. 1997). We then quantified the release of free cholesterol/cholesteryl ester into the medium upon SFN treatment in HeLa NPC1 cells using the Cholesterol/Cholesteryl Ester assay Kit. This assay allows to detect total cholesterol or free cholesterol in the presence or absence of cholesterol esterase; the levels of cholesteryl ester are determined by subtracting the levels of free cholesterol from total cholesterol. As shown in **Fig. 4C**, the levels of free cholesterol released into the medium treated were significantly increased with SFN (15 μM, 24 h) treatment compared to untreated control, suggesting that SFN can stimulate the release of free cholesterol into medium. Notably, the difference of released cholesteryl ester with or without SFN treatment has not been observed and the percentage of cholesteryl ester in total cholesterol released to medium were less than 10% under all conditions tested. Meanwhile, we further examined the effect of SFN on the release of lysosomal enzymes -β-hexosaminidase (NAGase) and acid phosphatase (ACP). In HeLa NPC1 cells treated with SFN (15 μM, 24 h), significantly higher levels of lysosomal enzymes (NAGases and ACP) were detected in the medium compared with untreated controls, but not in *TFEB* KO cells (**Fig. 4D**). Taken together, these results indicate that SFN induces an active movement of lysosomes toward the PM and increases lysosomal exocytosis in a TFEB-dependent manner.

Previously we reported that SFN could increase lysosome biogenesis and regulate lysosomal function, which contribute to ROS reduction in NPC models (Li, Shao et al. 2020). We then studied whether SFN activate lysosomal machinery in NPC1 cells. In HeLa NPC1 cells, SFN (15 μM, 12 h) treatment significantly increased the immunofluorescence intensity of LAMP1 (**Fig. 4E, F**). Likewise, similar results were observed in NPC1 KD cells (***Fig. S8A, B***). Lysosomal enzymes operate better under acidic conditions, and the degradation-active lysosomes can be tracked using LysoTracker, a fluorescent acidotropic probe (Li, Gu et al. 2019). We observed significant increases of LysoTracker staining in HeLa NPC1 cells following 12 h treatment with SFN (15 μM) (**Fig.**

4G, H) as well as in NPC1 KD cells (***Fig. S8C, D***), yet LAMP1 staining was also increased (**Fig. 4E, F; *Fig. S8A, B***). Thus lysosomal pH was more accurately determined using a ratiometric dye- pHrodo Green Dextran. When the fluorescence ratios (pHrodo Green Dextran /CF555) were calibrated to pH values, we found that SFN treatment induced significant lysosomal hyperacidity (**Fig. 4I, J**). Collectively, these results suggest that SFN promotes lysosome function and biogenesis in human NPC1 model cells, consistent with our previous report.

Notably, we then examined the TFEB expression in two NPC cell lines (HeLa NPC1 cells and NPC1-patient fibroblast cells). As shown in ***Fig. S9A, B***, TFEB expression levels in both NPC cell models were significantly decreased compared to WT, indicating that TFEB expression may be inhibited in NPC cells. Interestingly, the basal levels of lysosome biogenesis in NPC cells were comparable with WT cells (**Fig. 4D-G**, ***Fig. S8A-D***), suggestive of compensatory changes caused by TFEB downregulation. Taken together, excessive activation of TFEB in NPC cells can be targeted for cholesterol clearance via upregulation of lysosomal function and biogenesis.

SFN alleviates cholesterol accumulation in primary NPC1 $^{-/-}$ MEF cells

To address the possible relevance of the SFN/TFEB axis in NPC pathology of mice experiments, we then investigated whether SFN is sufficient to reduce cholesterol and regulates lysosomal function via TFEB activation in primary murine cells. Primary mouse embryonic fibroblasts (MEF) were freshly prepared from *NPC1$^{-/-}$* mice (from Jackson's laboratory). SFN (15 μM) treatment for 24 h dramatically increased TFEB nuclei signal in the *NPC1$^{-/-}$* MEF cells (**Fig. 5A, B**). Next, we analyzed the effect of SFN on cholesterol clearance in *NPC1$^{-/-}$* MEF cells. SFN (15 μM) treatment for 72 h exhibited substantial cholesterol reduction, whereas SFN treatment for 24 h showed relative weaker cholesterol clearance in MEF cells (**Fig. 5C, D**) compared with human NPC1 cells (**Fig. 1C**), suggesting that human NPC cells are more sensitive to SFN treatment compared to mouse NPC cells. We further tested whether SFN promotes lysosomal biogenesis and function in *NPC1$^{-/-}$* MEF cells. Following 24 h treatment with SFN (15 μM), a significant increase of LAMP1 staining (**Fig. 5E, F**) and LysoTracker intensity (**Fig. 5G, H**) were observed in *NPC1$^{-/-}$* MEF cells.

Collectively, these results suggest that SFN regulates TFEB-mediated lysosomal function axis and promotes cellular cholesterol clearance in NPC MEF cells.

SFN alleviates the loss of Purkinje cells and body weight in Npc1$^{-/-}$ mice

Considering that SFN promotes lysosomal cholesterol clearance in both human and murine NPC1 cell models (**Fig. 1**, **2**, **5**) and reportedly penetrates blood–brain barrier (BBB) (Kim, Kim et al. 2012, Mao, Yang et al. 2018, Tavakkoli, Iranshahi et al. 2019). We next investigated that whether SFN targets/activates TFEB in brain, 4-week-old BALB/cJ mice were intraperitoneally injected with SFN (50 mg/kg) or vehicle for 12 h and brain tissues including cerebellum and hippocampus were collected and pS211-TFEB/TFEB levels were measured by western blotting. As shown in **Fig. 6A**, **B**, we observed a significant decrease of pS211-TFEB protein in brain tissues with SFN treatment compared to vehicle, suggesting that TFEB in the brain was directly targeted by SFN treatment. This is the first time that SFN was shown to directly active TFEB in the brain. We then evaluated the *in vivo* therapeutic efficacy of SFN, *NPC1$^{-/-}$* mice (4-week-old) were treated with SFN (30 or 50 mg/kg) by daily intraperitoneal injection for 4 weeks. Purkinje cells located in the cerebellum are the most susceptible to NPC1 loss and exhibit significant selective loss in the anterior part of the cerebellum (Sarna, Larouche et al. 2003). Purkinje cells in cerebellum sections were stained by Calbindin and quantified by recording the number of surviving cells in lobules/mm of Purkinje cell layer. As shown in **Fig. 6C, D**, little survival of Purkinje cells in vehicle-treated *NPC1$^{-/-}$* cerebellum, in contrast, daily injection of SFN (50 mg/kg) in NPC1 mice prevented a degree of Purkinje cell loss particularly in the lobule IV/V of cerebellum. Body weight is another important indicator of therapeutic efficacy in NPC mice. Typically, NPC1 mice weight plateaus at 6-7 weeks of age, and then progressively declines. Notably, we observed that daily i.p. injection of SFN (50 mg/kg) exhibited a significantly improvement in weight loss of NPC1 mice (**Fig. 6E**). However, SFN treatment has no effect on liver and spleen enlargement of NPC1 mice (data not shown). Collectively, our results demonstrated that pharmacological activation of TFEB by small-molecule agonist can mitigate NPC neuropathological symptoms *in vivo*.

Discussion

We have demonstrated in the current study that genetic overexpression of TFEB, but not TFE3 can dramatically mitigate cholesterol accumulation in NPC cells. Pharmacological activation of TFEB by SFN, a previously identified TFEB agonist (Li, Shao et al. 2021), significantly promoted cholesterol clearance in human and mouse NPC cells, while genetic inhibition (KO) of TFEB blocked SFN-induced cholesterol clearance. This clearance effect exerted by SFN was associated with upregulated lysosomal exocytosis and biogenesis. Notably, SFN is reportedly BBB-permeable, assuring a good candidate for efficient delivery to the brain, which is essential for targeting neurodegenerative phenotypes in neurological diseases including NPC. In the NPC mouse models, SFN exhibits *in vivo* efficacy of suppressing the loss of Purkinje cells and maintaining body weight. Hence, genetically or pharmacologically targeting TFEB may represent a promising approach to treat NPC and manipulating lysosome function with small-molecule TFEB agonists may have broad therapeutic potentials.

The MiT/TFE family contains four factors: MITF, TFEB, TFE3, and TFEC, which share an identical basic region for DNA binding, and highly similar HLH and Zip regions for dimerization (Haq and Fisher 2011). Many of the mechanistic insights into MiT regulation have been focused on TFEB and TFE3, which shares some overlapping functions, Surprisingly, in this study we found that overexpression of TFEB, but not TFE3 alleviated lysosomal cholesterol accumulation in NPC cells (**Fig. 1A, B, *Fig. S1A, B***). Moreover, studies reported that only TFEB overexpression, but not other MiT members upregulates lysosomal gene expression (Sardiello, Palmieri et al. 2009). Thus, these results suggest that the functions exerted by TFEB and TFE3 in NPC may appear to be specialized.

As a proof of the role of TFEB activation in NPC, pharmacological activation of TFEB by SFN, a natural small-molecule TFEB agonist, promotes a dramatic lysosomal cholesterol-lowering effect in several genetic and pharmacological NPC cell models (**Fig. 1C, 5C**). The concentration of SFN used in this study has no cytotoxicity towards the cell lines we used (***Fig. S10***). SFN-induced lysosomal exocytosis and the increased population of lysosomes ready to fuse with the PM contribute to the cholesterol clearance by SFN (**Fig. 4A-G**). Previously we have shown that SFN can mitigate oxidative stress via a ROS-Ca^{2+}-

calcineurin-TFEB-mediated lysosomal function and autophagy flux (Li, Shao et al. 2021). SFN, an electrophilic compound enriched in cruciferous vegetables such as broccoli, is a known potent inducer of NFE2L2/NRF2 in various cell types including NPC cells (***Fig. S6A,B***), a transcriptional factor that controls the expression of multiple detoxifying enzymes through antioxidant response elements (AREs) (Yamamoto, Kensler et al. 2018). Notably, the promoter region of the *Nfe2l2* gene harbors a CLEAR site, and TFEB activation can upregulate the expression of *Nfe2l2* (Mansueto, Armani et al. 2017). Hence, TFEB, together with NFE2L2, function as key regulators of cellular redox. Oxidative stress is a major feature of NPC and has been attributed to neuronal damage, leading to the pathogenesis and progression of NPC (Vazquez, Balboa et al. 2012). Elevated oxidative stress has been observed in the brain of NPC patient and mice (Smith, Wallom et al. 2009, Zampieri, Mellon et al. 2009). NPC patients also show decreased antioxidant capacity (expressed as Trolox equivalents) and diminished activity of different antioxidant enzymes, which indicates a decrease in antioxidant defenses (Fu, Yanjanin et al. 2010). Hence, the protective effect of SFN against NPC could attribute to a combination with antioxidant activity and cholesterol clearance via the lysosome-dependent, TFEB-mediated regulation. Therefore, pharmacological activation of TFEB may serve as a potential therapeutic strategy for NPC.

Materials and Methods

Mammalian cell culture. HeLa cells were cultured in Dulbecco's Modified Eagle's Medium (DMEM; Thermo Fisher Scientific, 11195-065) supplemented with 10 % fetal bovine serum (FBS; Thermo Fisher Scientific, 10091148). NPC1 patient-derived fibroblast cells (clone GM03123) and a healthy control (clone GM03440) were obtained from the Coriell Institute for Medical Research (NJ, USA). Human fibroblast cells were maintained in modified Eagle's medium (Thermo Fisher Scientific, 1964643) supplemented with 15 % FBS, 2 mM glutamine (Thermo Fisher Scientific, 25030081) and 1 % penicillin-streptomycin. *NPC1*$^{-/-}$ MEF cells were cultured in DMEM with 10 % FBS, 1 % penicillin-streptomycin and 1 % antibiotic-antimycotic (Thermo Fisher Scientific, 15240062). Macrophage cells were cultured

in RPMI 1640 medium (Gibco, B122656) supplemented with 20 % FBS. Unless otherwise indicated, all cell cultures were maintained at 37 °C in a humidified 5 % CO_2 incubator.

Stable and CRISPR/Cas9 KO cell lines. GFP-TFEB stable HeLa cell line was kindly provided by Dr. Shawn Ferguson (Yale School of Medicine) (Zhang, Cheng et al. 2016). *TFEB* CRISPR-Cas9 KO HeLa cells were generated and characterized as reported previously (Li, Shao et al. 2020).

Plasmids/siRNA transfection. Plasmids including mCherry-TFEB, mCherry-TFEB^{S211A} and TFE3-GFP were maintained in our laboratory as previously described (Nezich, Wang et al. 2015, Li, Shao et al. 2021). The siRNA sequences targeting human *TFEB* (5□-GAA AGG AGA CGA AGG UUC AAC AUC A-3□) were purchased from Invitrogen. The siRNA sequences targeting human *NPC1* (5□-CAA UUG UGA UAG CAA UAU UTT-3□) were chemically synthesized by GenePharma (Shanghai, China). HeLa cells were transfected with plasmids or siRNA using Lipofectamine 3000 reagent (Thermo Fisher Scientific, 2163785) or RNAi-Max reagent (Thermo Fisher Scientific, 13778150) in Opti-MEM (Thermo Fisher Scientific, 11058021), respectively. The efficiency of transfection was examined by Western blotting or Q-PCR.

Filipin staining. Cellular unesterified cholesterol were detected using a cell-based cholesterol assay kit (Abcam, ab133116). It provides a simple fluorometric method to detect the interaction of cholesterol and filipin III, which alters the filipin absorption and fluorescence spectra allowing visualization with a fluorescence microscope. Cells were cultured at $5x10^2$ cells/well in black, clear-bottom 96-well plates and treated with compounds for the indicated conditions. After rinsing with PBS twice, cells were fixed with fixation solution for 10min followed by a PBS rinse twice. The cells were then stained with filipin III solution for 1 h at room temperature in the dark. The images were then captured by an Olympus IX73/Zeiss microscope. Image analysis was conducted using the image J software.

Immunofluorescence and confocal imaging. For immunofluorescence detection of TFEB

and Nrf2, cells were grown on coverslips, fixed with 4 % PFA, permeabilized with 0.3 % Triton X-100 (Solarbio, T8200), followed by blocking in 1 % bovine serum albumin (BSA, Merck, B2064) in PBS for 1 h. Cells were then incubated with anti-TFEB (Cell Signaling Technology, 4240) or anti-Nrf2 antibody (Abcam, ab623521) at 4 □ overnight. After four washes with PBS, coverslips were incubated with secondary antibodies for 1 h and counterstained with DAPI for 10 min. For LAMP1 immunostaining, cells were fixed with 100 % methanol (-20 °C) for 10 min and then blocked with 1 % BSA in PBS for 1 h. The primary anti-LAMP1 (Abcam, ab24170) was used in this study. Finally, coverslips were mounted with Fluoromount-G (Southern Biotech, 0100-01) and ready for imaging.

Western Blotting. Cells were lysed with ice-cold RIPA buffer (Solarbio, R0010) in the presence of 1×protease inhibitor cocktail (Merck, P8340) and 1×phosphatase inhibitor cocktail (Abcam, GR304037-28) on ice for 20 min. Cells were then centrifuged and the supernatant was collected. The protein concentration of the supernatant was determined using BCA Protein Assay (Thermo Scientific, UA269551). Protein samples (20-40 μg) were then loaded and separated on SDS-polyacrylamide gradient gels (GenScript, M00654) followed by the transfer to polyvinylidene difluoride membranes (Merck, R7DA8778E). Western blot analysis was performed using primary antibodies against TFEB (1:500, Cell Signaling Technology, 4240 for cells, 1:1000, Bethyl Laboratories, A303-673A for mice tissue), pS122-TFEB (1:500, Cell Signaling Technology, 86843), pS142-TFEB (1:500, Millipore, 3321796), pS211-TFEB (1:500, Cell Signaling Technology, 37681), NPC1 (1:1000, Abcam, ab134113), LAMP1 (1:500, Abcam, ab24170), MTOR (Cell Signaling Technology, 2972), p-MTOR (Sigma-Aldrich, SAB4504476), p-RPS6KB1/S6K1 (Cell Signaling Technology, 9234), RPS6KB1/S6K1 (Cell Signaling Technology, 2708), NPC1 (1:1000, Santacruz, sc271335) and GAPDH (1:10000, Sigma-Aldrich, G9545). Bound proteins were then detected with secondary antibodies against horseradish peroxidase-conjugated and enhanced chemiluminescence reagents (Thermo Fisher Scientific, 203-17071). The membranes were visualized by using an Li-COR Biosciences Odyssey Fc system and the band intensity was quantified using Image J software.

LAMP1 surface labeling. Cells were pretreated with SFN as indicated time. For the experiment of co-staining of DiO and surface LAMP1, cells were first incubated with 5 μM DiO (HY-D0969, MCE) at 37℃ for 30 min and washed with PBS twice to remove the unbound dye. Nonpermeabilized cells were then labeled with anti-human LAMP1 antibody (1:500, DSHB, H4A3), which recognizes a luminal epitope, at 4 °C for 1 h. Cells were then fixed in 2 % paraformaldehyde for 30 mins and incubated with Alexa Flour 488-conjugated secondary antibody at room temperature for 1 h. After PBS wash for three times, cells were counterstained with DAPI for 10 min and images were captured by Zeiss confocal microscope.

Lysosomal pH imaging. To measure lysosomal luminal pH, live cells were treated with chemicals as indicated condition, followed by incubation with 50 nM LysoTracker Red DND-99 (Thermo Scientific, L7528) for 15-30 min. Cells were then washed with PBS for three times. Images were captured by an Olympus/Zeiss microscope. Fluorescence intensities were quantified using the Image J software.

Lysosomal luminal acidity was also evaluated with the fluorescence ratio between a pH-sensitive dye pHrodo™ Green conjugated dextran-10 kd (P35368, Invitrogen) and a pH-insensitive dye CF555 conjugated dextran-10 kd (80112, Biotium). Briefly, cells were seeded on coverslips and loaded with 20 μg/mL of each dextran overnight. Cells were then chased in medium without dye for 3 hours before imaging. The HEPES buffered DMEM medium without phenol red (21063029, Gibco) was used as the imaging solution to eliminate the short time starvation side effects during imaging process. Cells were washed with the imaging solution and imaged using an inverted microscope (Olympus IX81). The fluorescence emission excited at 488 nm and 561 nm wavelengths were acquired with an EM-CCD camera. The fluorescence intensity of pHrodo™ Green and CF555 were quantified by Image J.

RNA extraction and RT-QPCR. Total RNA was extracted using TRIzol according the manufacturer's protocol (Thermo Scientific, 191002). cDNA was generated with 100-500 ng of total RNA using GoScript Reverse Transcription System (Promega, 0000316057). Q-PCR

was performed using SYBR Green (TOYOBO, 563700) in CFX Connect Optics (BIORAD). The changes in the mRNA expression of target genes were normalized to that of the housekeeping gene HPRT. Primer sequences used in this study are listed as following:

HPRT: For 5□- TGGCGTCGTGATTAGTGATG -3□, Rev 5□-CTGTTCTCGTCCAGCAGACACT -3□

LAMP1: For 5□-CGTGTCACGAAGGCGTTTTCAG -3□, Rev 5□-CTGTTCTCGTCCAGCAGACACT -3□

ULK1: For 5'-TCATCTTCAGCCACGCTGT-3', Rev 5'-CACGGTGCTGGAACATCTC-3'

SQSTM1: For 5□- CTGGGACTGAGAAGGCTCAC-3□; Rev 5□- GCAGCTGATGGTTTGGAAAT-3□

ATG5: For 5□- TGCGGTTGAGGCTCACTTTATGTC-3'; Rev 5□- GTCCCATCCAGAGCTGCTTGTG-3'

mGAPDH: For 5'-TGA ATA CGG CTA CAG CA -3'; Rev 5'-AGG CCC CTC CTG TTATTA TG-3'

mSQSTM1: For 5□-AGGAGGAGACGATGACTGGACAC-3'; Rev 5□-TTGGTCTGTAGGAGCCTGGTGAG-3'

mLC3: For 5□- CAAGCCTTCTTCCTCCTGGTGAATG-3'; Rev 5□-CCATTGCTGTCCCGAATGTCTCC-3'

mCTSF: 5□-ACGCCTATGCAGCCATAAAG -3'; Rev 5□-CTTTTGCCATCTGTGCTGAG-3'

Measurement of NAGase and ACP activity. Activities of NAGase and ACP enzymes were measured using microplate assay kits (NAGase, absin, abs580171; ACP, Solarbio, BC2135) respectively. Following the manufacturer's instructions, cells were seeded in 6-well plates and treated with chemicals in FBS-free medium as indicated condition. Aliquot of supernatant medium was collected and put on ice for extracellular (medium) enzyme activity detection. Cells were collected and 100 μl of assay buffer was added. The cell suspension was then sonicated and centrifuged for 8000 x *g* for 10 mins, supernatant was collected for cellular enzyme activity detection. NAGase activity was measured in a 96-well microtiter plate containing 25 μl of sample (medium or cell lysates) and 25 μl of substrate in each well, which was mixed and incubated at 37 °C for 20 mins, and then 50 μl of stop solution was added to stop the reaction. ACP activity was measured in a microtiter plate containing 20 μl of sample, 40 μl of Reagent □ and 40 μl of Reagent □. The plate was incubated at 37 °C for 15 min and then 120 μl of Reagent □ was added. Finally, the absorbance of NAGase /ACP was recorded at 405 nm/ 510 nm using a FlexStation 3 Multi-Mode microplate reader (Molecular Devices) respectively. NAGase /ACP activity released to medium (%) = Enzyme activity in medium / total enzyme activity (medium + cell lysates).

Detection of Cholesterol content. The levels of total and free cholesterol released in medium were measured using a colorimetric cholesterol/cholesteryl ester detection kit (Abcam, ab102515) according to the manufacturer's instructions. Briefly, aliquot of supernatant medium was collected and air-dried at 50 °C. The dried mixture was dissolved in cholesterol assay buffer. Aliquot of samples were mixed with cholesterol assay buffer, substrate and cholesterol enzyme with or without cholesterol esterase and incubated at 37 °C for 30 min. The absorbance was measured at 450 nm using a FlexStation 3 Multi-Mode microplate reader (Molecular Devices). The amount of cholesterol was calculated by standard curve and normalized with cellular protein content.

Cell viability assay. Cell viability was assessed by MTT assay (Merck, M2128-5G). A modified MTT assay was applied to measure the cell viability. Briefly, approximately 10^4 cells were seeded in 96-well plates and exposed to SFN as required. Cells were then incubated in fresh medium containing 0.2 mg/ml MTT solution for 4 h. The supernatant was removed and 100 μl of acidified DMSO (0.04 M HCl/DMSO) was added to dissolve the precipitation at 37 °C for 10 min. The absorbance of dissolved solution was measured at 490 nm with Flexstation® 3 (Molecular Devices). Cell mortality (%) was calculated by $(OD^{Control}-OD^{Sample})/OD^{Control} \times 100$.

Animals. *NPC1*$^{-/-}$ mice (BALB/cNctr-Npc1 m1N/J, also known as $NPC1^{NIH}$) were purchased from The Jackson Laboratory (USA). All the experimental procedures were conducted in accordance with the Guide for the Care and Use of Laboratory Animals in the Zhejiang University of Technology (Hangzhou, China) and conformed to the National Institutes of Health Guide for Care and Use of Laboratory Animals. Unless stated otherwise, mice were fed with free access to water and standard diet under specific pathogen-free conditions. Genotypes were identified using a PCR-based screening (Amigo, Mendoza et al. 2002).

Histological analysis. Mice perfusion was performed with PBS. Then, mice cerebellums were post-fixed overnight at 4 °C and after this, placed in serial dilutions of sucrose (10-30 %) in PBS at 4°C overnight, respectively. Then cerebellums were cut in 5 μM thick sagittal

sections by cryostat at (Leika) at -20 °C. Permeabilized slices with 0.1 % Triton X-100 were blocked in 1 % BSA in PBS for 1 h. Slices were incubated with anti-calbindin (Abcam, 108404) overnight at 4 °C and followed by incubation with the secondary antibody conjugated with Alexa Fluor 488 for 2 h. The slices were then washed with PBS three times and incubated with DAPI in dark for 10 min. All the images were captured by an Olympus or Zeiss confocal microscope.

Isolation of Primary MEF and macrophage cells. MEF cells were prepared from neonatal mice, which were euthanized by CO_2. Skin of neonatal mice were cut with scissors and gently clipped and added to 0.25 % trypsin-EDTA in the 37 °C incubator for 20 min. The cell suspension was then transferred to a 50 ml tube and 10 ml of DMEM media was added to inactivate the trypsin reaction for 5 min. The supernatant was transferred to a 60 mm dish and keep in incubator at 37 °C for 3 h, then the medium was replaced by DMEM with 10 % FBS, 1 % penicillin/streptomycin until confluency (2 to 4 days). Primary macrophages were established from hindlimb femurs and tibias of newborn mice. The marrow cells were flushed from the bones with PBS and centrifuged. Cells were then resuspended in RPMI 1640 medium (Gibco, B122656) supplemented with 20 % FBS. Cells were then seeded in culture dishes coated with 2 % gelatin and allowed to adhere for 2 h at 37 ℃.

Reagents. Chemicals used in this study including SFN (Sigma-Aldrich, S4441), DMSO (Sigma-Aldrich, D2660), Filipin III (Cayman Chemical, 70440), U18666A (MedChemExpress, HY-107433), Triton X-100 (MCE, HY-Y1883A), NAC (Sigma-Aldrich, A7250), FK506 (Sigma-Aldrich, F4679), CsA (Solarbio, C8780), BAPTA-AM (Thermo Scientific, 1824047).

Data analysis. Data are presented as mean ± s.e.m. from at least 3 independent experiments. Statistical comparisons were performed with analyzes of variance (ANOVA) or Student's *t-test* with paired or unpaired wherever appropriate. A p value < 0.05 was considered as statistically significant.

Acknowledgement

This work was supported by a NSFC grant (31600823 to D. L). Additional support was provided by Calygene Biotechnology Inc. (XT [2016]008@). The funders had no role in study design**,** data collection and analysis, decision to publish, or preparation of the manuscript. We are grateful to Dr. Shawn M. Ferguson for the GFP-TFEB stable cells and Dr. Haoxing Xu for the *TFEB* KO cells.

Disclosure statement

No potential conflict of interest was reported by the authors.

References

Amigo, L., H. Mendoza, J. Castro, V. Quinones, J. F. Miquel and S. Zanlungo (2002). "Relevance of Niemann-Pick type C1 protein expression in controlling plasma cholesterol and biliary lipid secretion in mice." Hepatology **36**(4 Pt 1): 819-828.

Argüello, G., E. Balboa, P. J. Tapia, J. Castro, M. J. Yañez, P. Mattar, R. Pulgar and S. Zanlungo (2021). "Genistein Activates Transcription Factor EB and Corrects Niemann-Pick C Phenotype." Int J Mol Sci **22**(8).

Ballabio, A. (2016). "The awesome lysosome." EMBO Mol Med **8**(2): 73-76.

Carstea, E. D., J. A. Morris, K. G. Coleman, S. K. Loftus, D. Zhang, C. Cummings, J. Gu, M. A. Rosenfeld, W. J. Pavan, D. B. Krizman, J. Nagle, M. H. Polymeropoulos, S. L. Sturley, Y. A. Ioannou, M. E. Higgins, M. Comly, A. Cooney, A. Brown, C. R. Kaneski, E. J. Blanchette-Mackie, N. K. Dwyer, E. B. Neufeld, T. Y. Chang, L. Liscum, J. F. Strauss, 3rd, K. Ohno, M. Zeigler, R. Carmi, J. Sokol, D. Markie, R. R. O'Neill, O. P. van Diggelen, M. Elleder, M. C. Patterson, R. O. Brady, M. T. Vanier, P. G. Pentchev and D. A. Tagle (1997). "Niemann-Pick C1 disease gene: homology to mediators of cholesterol homeostasis." Science **277**(5323): 228-231.

Chien, Y. H., S. F. Peng, C. C. Yang, N. C. Lee, L. K. Tsai, A. C. Huang, S. C. Su, C. C. Tseng and W. L. Hwu (2013). "Long-term efficacy of miglustat in paediatric patients with Niemann-Pick disease type C." J Inherit Metab Dis **36**(1): 129-137.

Corssac, G. B., C. Campos-Carraro, A. Hickmann, A. S. da Rosa Araujo, R. O. Fernandes and A. Belló-Klein (2018). "Sulforaphane effects on oxidative stress parameters in culture of adult cardiomyocytes." Biomedicine & Pharmacotherapy **104**: 165-171.

Davis, O. B., H. R. Shin, C. Y. Lim, E. Y. Wu, M. Kukurugya, C. F. Maher, R. M. Perera, M. P. Ordonez and R. Zoncu (2021). "NPC1-mTORC1 Signaling Couples Cholesterol Sensing to Organelle Homeostasis and Is a Targetable Pathway in Niemann-Pick Type C." Dev Cell **56**(3): 260-276.

Decressac, M. and A. Björklund (2013). "TFEB: Pathogenic role and therapeutic target in Parkinson disease." Autophagy **9**(8): 1244-1246.

Fraldi, A., A. D. Klein, D. L. Medina and C. Settembre (2016). "Brain Disorders Due to Lysosomal Dysfunction." Annu Rev Neurosci **39**: 277-295.

Fu, R., N. M. Yanjanin, S. Bianconi, W. J. Pavan and F. D. Porter (2010). "Oxidative stress in Niemann-Pick disease, type C." Mol Genet Metab **101**(2-3): 214-218.

Giatromanolaki, A., D. Kalamida, E. Sivridis, I. V. Karagounis, K. C. Gatter, A. L. Harris and M. I. Koukourakis (2015). "Increased expression of transcription factor EB (TFEB) is associated with autophagy, migratory phenotype and poor prognosis in non-small cell lung cancer." Lung Cancer **90**(1): 98-105.

Haq, R. and D. E. Fisher (2011). "Biology and clinical relevance of the micropthalmia family of transcription factors in human cancer." J Clin Oncol **29**(25): 3474-3482.

Hoglinger, D., T. Burgoyne, E. Sanchez-Heras, P. Hartwig, A. Colaco, J. Newton, C. E. Futter, S. Spiegel, F. M. Platt and E. R. Eden (2019). "NPC1 regulates ER contacts with endocytic organelles to mediate cholesterol egress." Nat Commun **10**(1): 4276.

Kim, H. V., H. Y. Kim, H. Y. Ehrlich, S. Y. Choi, D. J. Kim and Y. Kim (2012). "Amelioration of Alzheimer's disease by neuroprotective effect of sulforaphane in animal model." Amyloid **20**(1): 7-12.

Lange, Y. and T. L. Steck (1994). "Cholesterol homeostasis. Modulation by amphiphiles." J Biol Chem **269**(47): 29371-29374.
Levine, B. and G. Kroemer (2008). "Autophagy in the pathogenesis of disease." Cell **132**(1): 27-42.
Li, D., R. Shao, N. Wang, N. Zhou, K. Du, J. Shi, Y. Wang, Z. Zhao, X. Ye, X. Zhang and H. Xu (2020). "Sulforaphane Activates a lysosome-dependent transcriptional program to mitigate oxidative stress." Autophagy **15**: 1-16.
Li, D., R. Shao, N. Wang, N. Zhou, K. Du, J. Shi, Y. Wang, Z. Zhao, X. Ye, X. Zhang and H. Xu (2021). "Sulforaphane Activates a lysosome-dependent transcriptional program to mitigate oxidative stress." Autophagy **17**(4): 872-887.
Li, P., M. Gu and H. Xu (2019). "Lysosomal Ion Channels as Decoders of Cellular Signals." Trends Biochem Sci **44**(2): 110-124.
Liao, G., Z. Wang, E. Lee, S. Moreno, O. Abuelnasr, M. Baudry and X. Bi (2015). "Enhanced expression of matrix metalloproteinase-12 contributes to Npc1 deficiency-induced axonal degeneration." Exp Neurol **269**: 67-74.
Liu, Y., X. Fu, Z. Chen, T. Luo, C. Zhu, Y. Ji and Z. Bian (2021). "The Protective Effects of Sulforaphane on High-Fat Diet-Induced Obesity in Mice Through Browning of White Fat." Frontiers in Pharmacology **12**.
Lu, F., Q. Liang, L. Abi-Mosleh, A. Das, J. K. De Brabander, J. L. Goldstein and M. S. Brown (2015). "Identification of NPC1 as the target of U18666A, an inhibitor of lysosomal cholesterol export and Ebola infection." Elife **4**.
Mansueto, G., A. Armani, C. Viscomi, L. D'Orsi, R. De Cegli, E. V. Polishchuk, C. Lamperti, I. Di Meo, V. Romanello, S. Marchet, P. K. Saha, H. Zong, B. Blaauw, F. Solagna, C. Tezze, P. Grumati, P. Bonaldo, J. E. Pessin, M. Zeviani, M. Sandri and A. Ballabio (2017). "Transcription Factor EB Controls Metabolic Flexibility during Exercise." Cell Metab **25**(1): 182-196.
Mao, L., T. Yang, X. Li, X. Lei, Y. Sun, Y. Zhao, W. Zhang, Y. Gao, B. Sun and F. Zhang (2018). "Protective effects of sulforaphane in experimental vascular cognitive impairment: Contribution of the Nrf2 pathway." Journal of Cerebral Blood Flow & Metabolism **39**(2): 352-366.
Martina, J. A., Y. Chen, M. Gucek and R. Puertollano (2012). "MTORC1 functions as a transcriptional regulator of autophagy by preventing nuclear transport of TFEB." Autophagy **8**(6): 903-914.
Martina, J. A. and R. Puertollano (2018). "Protein phosphatase 2A stimulates activation of TFEB and TFE3 transcription factors in response to oxidative stress." J Biol Chem **293**(32): 12525-12534.
Martina, J. A. and P. Rosa (2018). "Protein phosphatase 2A stimulates activation of TFEB and TFE3 transcription factors in response to oxidative stress." Journal of Biological Chemistry **293**: jbc.RA118.003471-.
Martini-Stoica, H., Y. Xu, A. Ballabio and H. Zheng (2016). "The Autophagy-Lysosomal Pathway in Neurodegeneration: A TFEB Perspective." Trends Neurosci **39**(4): 221-234.
Medina, L. Diego, P. Di, Simone, Peluso, Ivana, Armani, Andrea, D. Stefani and Diego "Lysosomal calcium signalling regulates autophagy through calcineurin and TFEB."
Medina, D. L., A. Fraldi, V. Bouche, F. Annunziata, G. Mansueto, C. Spampanato, C. Puri, A. Pignata, J. A. Martina, M. Sardiello, M. Palmieri, R. Polishchuk, R. Puertollano and A.

Ballabio (2011). "Transcriptional activation of lysosomal exocytosis promotes cellular clearance." Dev Cell **21**(3): 421-430.
Napolitano, G. and A. Ballabio (2016). "TFEB at a glance." J Cell Sci **129**(13): 2475-2481.
Napolitano, G., A. Esposito, H. Choi, M. Matarese, V. Benedetti, C. Di Malta, J. Monfregola, D. L. Medina, J. Lippincott-Schwartz and A. Ballabio (2018). "mTOR-dependent phosphorylation controls TFEB nuclear export." Nat Commun **9**(1): 3312.
Nezich, C. L., C. Wang, A. I. Fogel and R. J. Youle (2015). "MiT/TFE transcription factors are activated during mitophagy downstream of Parkin and Atg5." J Cell Biol **210**(3): 435-450.
Pineda, M., M. S. Perez-Poyato, M. O'Callaghan, M. A. Vilaseca, M. Pocovi, R. Domingo, L. R. Portal, A. V. Pérez, T. Temudo, A. Gaspar, J. J. Peñas, S. Roldán, L. M. Fumero, O. B. de la Barca, M. T. Silva, J. Macías-Vidal and M. J. Coll (2010). "Clinical experience with miglustat therapy in pediatric patients with Niemann-Pick disease type C: a case series." Mol Genet Metab **99**(4): 358-366.
Pineda, M., J. E. Wraith, E. Mengel, F. Sedel, W. L. Hwu, M. Rohrbach, B. Bembi, M. Walterfang, G. C. Korenke, T. Marquardt, C. Luzy, R. Giorgino and M. C. Patterson (2009). "Miglustat in patients with Niemann-Pick disease Type C (NP-C): a multicenter observational retrospective cohort study." Mol Genet Metab **98**(3): 243-249.
Poh, M. K., G. Shui, X. Xie, P. Y. Shi, M. R. Wenk and F. Gu (2012). "U18666A, an intra-cellular cholesterol transport inhibitor, inhibits dengue virus entry and replication." Antiviral Res **93**(1): 191-198.
Polito, V. A., H. Li, H. Martini-Stoica, B. Wang, L. Yang, Y. Xu, D. B. Swartzlander, M. Palmieri, A. di Ronza, V. M. Lee, M. Sardiello, A. Ballabio and H. Zheng (2014). "Selective clearance of aberrant tau proteins and rescue of neurotoxicity by transcription factor EB." EMBO Mol Med **6**(9): 1142-1160.
Puertollano, R., S. M. Ferguson, J. Brugarolas and A. Ballabio (2018). "The complex relationship between TFEB transcription factor phosphorylation and subcellular localization." EMBO J **37**(11).
Reddy, A., E. V. Caler and N. W. Andrews (2001). "Plasma membrane repair is mediated by Ca(2+)-regulated exocytosis of lysosomes." Cell **106**(2): 157-169.
Rodriguez, A., P. Webster, J. Ortego and N. W. Andrews (1997). "Lysosomes behave as Ca2+-regulated exocytic vesicles in fibroblasts and epithelial cells." J Cell Biol **137**(1): 93-104.
Sardiello, M. and A. Ballabio (2009). "Lysosomal enhancement: a CLEAR answer to cellular degradative needs." Cell Cycle **8**(24): 4021-4022.
Sardiello, M., M. Palmieri, A. di Ronza, D. L. Medina, M. Valenza, V. A. Gennarino, C. Di Malta, F. Donaudy, V. Embrione, R. S. Polishchuk, S. Banfi, G. Parenti, E. Cattaneo and A. Ballabio (2009). "A gene network regulating lysosomal biogenesis and function." Science **325**(5939): 473-477.
Sarkar, S., B. Carroll, Y. Buganim, D. Maetzel, A. H. Ng, J. P. Cassady, M. A. Cohen, S. Chakraborty, H. Wang, E. Spooner, H. Ploegh, J. Gsponer, V. I. Korolchuk and R. Jaenisch (2013). "Impaired autophagy in the lipid-storage disorder Niemann-Pick type C1 disease." Cell Rep **5**(5): 1302-1315.
Sarna, J. R., M. Larouche, H. Marzban, R. V. Sillitoe, D. E. Rancourt and R. Hawkes (2003). "Patterned Purkinje cell degeneration in mouse models of Niemann-Pick type C disease." J Comp Neurol **456**(3): 279-291.

Settembre, C., C. Di Malta, V. A. Polito, M. G. Arencibia, F. Vetrini, S. Erdin, S. U. Erdin, T. Huynh, D. Medina, P. Colella, M. Sardiello, D. C. Rubinsztein and A. Ballabio (2011). "TFEB Links Autophagy to Lysosomal Biogenesis." Science **332**(6036): 1429-1433.

Smith, D., K. L. Wallom, I. M. Williams, M. Jeyakumar and F. M. Platt (2009). "Beneficial effects of anti-inflammatory therapy in a mouse model of Niemann-Pick disease type C1." Neurobiol Dis **36**(2): 242-251.

Spampanato, C., E. Feeney, L. Li, M. Cardone, J. A. Lim, F. Annunziata, H. Zare, R. Polishchuk, R. Puertollano, G. Parenti, A. Ballabio and N. Raben (2013). "Transcription factor EB (TFEB) is a new therapeutic target for Pompe disease." EMBO Mol Med **5**(5): 691-706.

Tavakkoli, A., M. Iranshahi, S. H. Hasheminezhad, A. W. Hayes and G. Karimi (2019). "The neuroprotective activities of natural products through the Nrf2 upregulation." Phytotherapy Research **33**(9): 2256-2273.

Tsunemi, T. and A. R. La Spada (2012). "PGC-1α at the intersection of bioenergetics regulation and neuron function: from Huntington's disease to Parkinson's disease and beyond." Prog Neurobiol **97**(2): 142-151.

Tsunemi, T., T. Perez-Rosello, Y. Ishiguro, A. Yoroisaka, S. Jeon, K. Hamada, M. Rammonhan, Y. C. Wong, Z. Xie, W. Akamatsu, J. R. Mazzulli, D. J. Surmeier, N. Hattori and D. Krainc (2019). "Increased Lysosomal Exocytosis Induced by Lysosomal Ca(2+) Channel Agonists Protects Human Dopaminergic Neurons from alpha-Synuclein Toxicity." J Neurosci **39**(29): 5760-5772.

Vazquez, M. C., E. Balboa, A. R. Alvarez and S. Zanlungo (2012). "Oxidative stress: a pathogenic mechanism for Niemann-Pick type C disease." Oxid Med Cell Longev **2012**: 205713.

Wang, W., Q. Gao, M. Yang, X. Zhang, L. Yu, M. Lawas, X. Li, M. Bryant-Genevier, N. T. Southall, J. Marugan, M. Ferrer and H. Xu (2015). "Up-regulation of lysosomal TRPML1 channels is essential for lysosomal adaptation to nutrient starvation." Proc Natl Acad Sci U S A **112**(11): E1373-1381.

Wraith, J. E., D. Vecchio, E. Jacklin, L. Abel, H. Chadha-Boreham, C. Luzy, R. Giorgino and M. C. Patterson (2010). "Miglustat in adult and juvenile patients with Niemann-Pick disease type C: long-term data from a clinical trial." Mol Genet Metab **99**(4): 351-357.

Xu, H. and D. Ren (2015). "Lysosomal physiology." Annu Rev Physiol **77**: 57-80.

Xu, Y., S. Du, J. A. Marsh, K. Horie, C. Sato, A. Ballabio, C. M. Karch, D. M. Holtzman and H. Zheng (2020). "TFEB regulates lysosomal exocytosis of tau and its loss of function exacerbates tau pathology and spreading." Mol Psychiatry.

Yamamoto, M., T. W. Kensler and H. Motohashi (2018). "The KEAP1-NRF2 System: a Thiol-Based Sensor-Effector Apparatus for Maintaining Redox Homeostasis." Physiol Rev **98**(3): 1169-1203.

Zampieri, S., S. H. Mellon, T. D. Butters, M. Nevyjel, D. F. Covey, B. Bembi and A. Dardis (2009). "Oxidative stress in NPC1 deficient cells: protective effect of allopregnanolone." J Cell Mol Med **13**(9B): 3786-3796.

Zhang, X., X. Cheng, L. Yu, J. Yang, R. Calvo, S. Patnaik, X. Hu, Q. Gao, M. Yang, M. Lawas, M. Delling, J. Marugan, M. Ferrer and H. Xu (2016). "MCOLN1 is a ROS sensor in lysosomes that regulates autophagy." Nat Commun **7**: 12109.

Figure Legends

Figure 1. TFEB overexpression or pharmacological activation of TFEB ameliorates cholesterol accumulation in U18666A-induced HeLa NPC1 model. (A) Overexpression of TFEB/ TFEB ^{S211A} reduced cellular cholesterol levels in U18666A-induced HeLa NPC1 model. Filipin staining of HeLa transiently transfected by mCherry, mCherry-TFEB and mCherry- TFEB ^{S211A} plasmid for 48 h, followed by U18666A (2.5 μM) for 24 h. Overlay phase contrast images are shown together with the red (mCherry-TFEB/TFEB ^{S211A}) and white (filipin). In each image the red circles point to the successful transfected cells, green circles represent the untransfected cells, Scale bar, 20 μm. **(B)** Quantification of cholesterol accumulation from **A.** N=30 randomly selected cells from *n*=3 independent experiments. **(C)** SFN reduces lysosomal (LAMP1) cholesterol accumulation (Filipin) in HeLa NPC1 cells. HeLa cells were exposed to U18666A (2.5 μM) in the absence or the presence of SFN (15 μM) for 24 h. Each panel shows fluorescence images taken by confocal microscopes. The red signal is LAMP1-mCherry driven by stable transfection, and the green signal is Filipin. **(D)** Each panel shows the fluorescence intensity of a line scan (white line on the blown-up image) through the double labeled object indicated by the white arrow. Scale bar, 20 μm or 2 μm (for zoom-in images). **(E)** Quantification of cholesterol levels shown in **C**. N=15 randomly selected cells from *n*=3 experiments. **(F)** SFN (15 μM, 24 h) induced TFEB nuclear translocation in HeLa NPC1 cells. Nuclei were counterstained with DAPI (blue). Scale bar, 20 μm. **(G)** Average ratios of nuclear vs. cytosolic TFEB immunoreactivity shown in **F**. N=20 randomly selected cells from *n*=3 experiments. **(H)** SFN induced mRNA expression of TFEB target genes in HeLa NPC1 model. HeLa cells were cotreated with U18666A (2.5 μM) and SFN (15 μM) for 24 h (*n*=3). **(I)** Western blot analysis of TFEB phosphorylation by SFN (15 μM, 24 h) in HeLa NPC1 cells. (**J**) Quantification of ratios of pS211-, pS142-, pS122-TFEB vs. total TFEB as shown in **I**. (*n*=3). For all the panels, average data are presented as mean **±** s.e.m.; *** $P < 0.001$.

Figure 2. SFN promotes cholesterol clearance in various human NPC1 cell models. (A) Western blot analysis of the KD efficiency of a specific NPC1-targeting siRNA in HeLa cells (n = 3 independent repeats). **(B)** SFN induced TFEB nuclear translocation in NPC1 KD HeLa

cells. Detection of TFEB immunoreactivity in HeLa cells transiently transfected with si*NPC1* for 48 h, followed by SFN (15 μM) treatment for 24 h. Scale bar, 20 μm. **(C)** Average ratios of nuclear vs. cytosolic TFEB immunoreactivity shown in **B**. N=20 randomly selected cells from 3 independent repeats. **(D)** In NPC1 KD HeLa cells, SFN (15 μM, 24 h) upregulated expression of TFEB target genes (*n*=3 independent repeats). **(E)** SFN promoted cholesterol clearance in NPC1 KD HeLa cells. HeLa cells was transiently transfected by si*NPC1* for 48 h, followed by SFN (15 μM) treatment for 24 h. Scale bar, 20 μm. **(F)** Quantification of cholesterol accumulation in NPC1 KD HeLa cells shown in **E**. N=15 randomly selected cells from 3 independent repeats. **(G)** SFN (15 μM, 24 h)-induced TFEB nuclear translocation in human NPC1 fibroblasts. Nuclei were counterstained with DAPI (blue). Scale bar, 20 μm. **(H)** Quantification of nuclear vs. cytosolic TFEB ratio as shown in **G**. N=20 randomly selected cells from at least 3 independent experiments. **(I)** SFN promoted cholesterol clearance in human NPC1-patient fibroblasts. Human NPC1 fibroblasts were treated with SFN (15 μM, 24 h) and filipin staining was carried out. Scale bar, 20 μm. **(J)** Quantification of cholesterol accumulation as shown in **I**. N=30 randomly selected cells from 3 independent repeats. For all the panels, average data are presented as mean **±** s.e.m.; *** $P < 0.001$.

Figure 3. TFEB is required for SFN-promoted cholesterol clearance. (A) Western blot analysis of the efficiency of si*TFEB* KD and mCherry-TFEB OE in HeLa cells. **(B)** HeLa cells were transfected with si*TFEB* or mCherry-TFEB for 48 h, followed by cotreatment with U18666A (2.5 μM) and SFN (15 μM) for 24 h and cholesterol accumulation was analyzed by Filipin assay. Scale bar, 20 μm. **(C)** Quantification of cholesterol levels as shown in **B**. N=15 randomly selected cells from 3 independent repeats. **(D)** Western blot analysis the efficiency of *TFEB* KO in HeLa cells. **(E)** HeLa, HeLa *TFEB* KO and HeLa *TFEB* KO cells transient expressing mCherry-TFEB (TFEB OE, 48 h) were cotreatment with U18666A (2.5 μM) and SFN (15 μM) for 24 h and cholesterol levels were analyzed by filipin assay. Scale bar, 20 μm. **(F)** Quantification analysis of cholesterol accumulation as shown in **E**. N=15 randomly selected cells from at least 3 independent experiments. Average data are presented as mean ± s.e.m.; ***$P < 0.001$.

Figure 4. SFN promotes lysosomal exocytosis and biogenesis in NPC1 cell models. (A) Confocal microscopy images showing the exposure of LAMP1 on the PM in nonpermeabilized HeLa NPC1 cells treated with SFN (15 μM) for 24 h using an antibody against LAMP1 luminal portion. Nuclei were counterstained with DAPI (blue). Scale bar, 20 μm. **(B)** Quantitative analysis of LAMP1 levels on the PM in HeLa NPC1 cells shown in **A**. Bars represent the fold increase of LAMP1 fluorescence on PM in SFN treated cells. N=15 randomly selected cells from 3 independent repeats. **(C)** SFN increased the release of free cholesterol into medium. HeLa cells were cotreated with U18666A (2.5 μM) and SFN (15 μM) for 24 h, and then examined for cholesterol. The levels of cholesterol in the medium or cell lysates were measured by cholesterol assay in a reaction mixture with (measuring total cholesterol content) or without (measuring free cholesterol content) cholesterol esterase enzyme (n=6 independent repeats). **(D)** SFN increased the release of lysosomal enzyme NAGases and ACP in HeLa NPC1 cells. HeLa cells were cotreated with U18666A (2.5 μM) and SFN for 24 h, and the activities of NAGases and ACP were analyzed in the medium and cell lysates (n=6 independent repeats). **(E)** LAMP1 staining in HeLa cells upon U18666A treatment (2.5 μM) in the presence and absence of SFN (15 μM). Nuclei were counterstained with DAPI (blue). Scale bar, 20 μm. **(F)** Quantification analysis of LAMP1 immunofluorescence shown in **E**. N=20 randomly selected cells from at least 3 independent experiments. **(G)** Effects of SFN on lysosome acidity. HeLa cells were treated with 2.5 μM U18666A (24 h) in the presence and absence of 15 μM SFN (12 h) and lysosomal pH was analyzed by LysoTracker Red DND-99 (50 nM). Scale bar, 20 μm. **(H)** Quantification of LysoTracker intensity shown in **G**. N=20 randomly selected cells from at least 3 independent experiments. **(I)** Effects of SFN on lysosomal acidity using a ratiometric pH dye. HeLa cells were treated with U18666A (2.5 μM) in the presence and absence of SFN (15 μM), lysosomal pH was determined using a ratiometric pH dye combination (pHrodo Green dextran and CF555 dextran). Scale bar, 20 μm or 2 μm (for zoom-in images). **(J)** Quantification analysis of lysosomal pH shown in **I**. Randomly selected cells from at least 3 independent experiments. For all the panels, data are presented as mean **±** s.e.m.; $^{**}P < 0.01$, $^{***}P < 0.001$.

Figure 5. SFN ameliorates cholesterol accumulation in *Npc1*$^{-/-}$ MEF cells. **(A)** SFN (15 μM) treatment induced TFEB nuclear translocation in NPC1 MEF cells. Nuclei were counterstained with DAPI (blue). Scale bar, 20 μm. **(B)** Average ratios of nuclear vs. cytosolic TFEB immunoreactivity shown in **A**. N=20 from 3 independent repeats. **(C)** SFN (15 μM, 24-72 h) reduced cholesterol accumulation in NPC1 MEF cells by filipin assay. Scale bar, 20 μm. **(D)** Quantification analysis of cholesterol accumulation levels shown in **C**. N=15 randomly selected cells from at least 3 independent experiments. **(E)** Effects of SFN (15 μM, 12 h) on intensity of LAMP1 in NPC1 MEF cells. Scale bar, 20 μm. **(F)** Quantification of LAMP1 intensity shown in **E**. N=20 randomly selected cells from at least 3 independent experiments. **(G)** Effects of SFN (15 μM, 12 h) on lysosome acidity in MEF cells. Scale bar, 20 μm. **(H)** Quantification analysis of LysoTracker intensity shown in **G**. N=20 randomly selected cells from at least 3 independent experiments. For all the panels, data are presented as mean ± s.e.m.; $^{*}P < 0.05$, $^{**}P < 0.01$, $^{***}P < 0.001$.

Figure 6. SFN rescues the loss of Purkinje cells and body weight in NPC *in vivo* model. mice. **(A)** SFN promoted TFEB dephosphorylation in mice brain. 4-week-old BALB/cJ mice were intraperitoneally (i.p) injected with SFN (50 mg/kg) or vehicle for 12 h and brain tissues including cerebellum and hippocampus were collected and subjected to detect pS211-TFEB and total TFEB levels by Western blotting. (**B**) Quantification of the ratios of p-TFEB vs. total TFEB as shown in **A.** (**C**) Cerebella from vehicle and SFN treated NPC mice were analyzed at 8 weeks of age for calbindin by immunohistochemistry. SFN and vehicle were intraperitoneally injected daily in 4-week-old NPC mice for 4 weeks. Scale bar = 200 μm. (n=6 for each group). **(D)** Quantification of the number of Purkinje cells as indicated in the anterior lobules (II-V) as shown in **C**. **(E)** Body Weight was registered during the treatment. For all the panels, data are presented as mean ± s.e.m.; $^{**}P < 0.01$, $^{***}P < 0.001$.

Figure 7. A working scheme to illustrate that small-molecule TFEB agonist promotes cholesterol clearance in NPC model via TFEB-upregulated lysosomal exocytosis and biogenesis. Pharmacological or genetic activation/overexpression of TFEB dramatically ameliorates cholesterol accumulation in NPC1 cells. Small-molecule, BBB-permeable TFEB

agonist-SFN induces TFEB nuclear translocation by dephosphorylation of TFEB at S142 and S211 residues, promoting lysosomal biogenesis and exocytosis, resulting in mitigating lysosomal cholesterol levels.

Supplementary Figure Legends

Figure S1. The effect of TFE3 overexpression on lysosomal cholesterol levels in HeLa NPC1 model. **(A)** HeLa cells were transiently transfected with TFE3-GFP plasmid for 48 h, followed by U18666A (2.5 μM, 24 h) treatment and Filipin staining was carried out. Overlay phase contrast images are shown together with the green (TFEB-GFP) and white (filipin). In each image the red circles point to the successful transfected cells, green circles represent the untransfected cells, Scale bar, 20 μm. **(B)** Quantification of cholesterol levels in untransfected and TFEB-GFP-transfected cells from **A**. N=15 randomly selected cells from *n*=3 independent experiments. Data are presented as mean ± s.e.m.

Figure S2. Filipin signal is not colocalized with ER marker calnexin in HeLa NPC1 cells. (A) HeLa cells were exposed to U18666A (2.5 μM) in the absence or the presence of SFN (15 μM) for 24 h. Each panel shows fluorescence images taken by confocal microscopes. The red signal is calnexin (ER marker), and the green signal is Filipin. **(B)** The graph shows the fluorescence intensity of a line scan (white line on the blown-up image) through the double labeled object indicated by the white arrow. **(C)** SFN reduces cholesterol accumulation in HeLa NPC1 cells. HeLa cells were cotreated with U18666A (2.5 μM) and SFN (15 μM) for 12-24 h and stained with filipin. Scale bar, 20 μm. **(D)** Quantification of cholesterol levels shown in **C**. N=15 randomly selected cells from *n*=3 experiments. Data are presented as mean ± s.e.m.; *** $P < 0.001$.

Figure S3. SFN-induced TFEB nuclear translocation via a ROS-Ca^{2+}-calcineurin pathway in HeLa NPC1 cells. The effect of FK506 (5 μM) + CsA (10 μM), BAPTA-AM (10 μM) or NAC (5 mM) pretreatment on SFN (15 μM, 4 h)-mediated TFEB nuclear translocation in HeLa NPC1 cells. Scale bar: 10 μm.

Figure S4. Western blot analysis of the phosphorylation status of MTOR and RPS6KB1 by SFN. (A) HeLa cells were co-treated with U18666A (2.5 μM) and SFN (15 μM) for 24 h. Then MTOR and RPS6KB1 activity were detected via ratios of p-MTOR vs. total MTOR and p-RPS6KB1 vs. total RPS6KB1 by Western blotting. **(B)** Quantification of the results shown in **A**. from n = 3 independent experiments. Data are presented as mean ± s.e.m..

Figure S5. Western blot analysis of NPC1 expression in human NPC1 patient fibroblasts. Human NPC1-patient fibroblasts were treated with SFN (15 μM) for 24 h, then the expression levels of NPC1 protein were detected by Western blotting.

Figure S6. SFN induced Nrf2 nuclear translocation in NPC cells. SFN (15 μM, 4 h) induced Nrf2 translocation from cytosol to nuclei in **(A)** HeLa NPC1 and **(B)** $NPC^{-/-}$MEF cells. Nuclei were counterstained with DAPI (blue). Scale bar: 10 μm.

Figure S7. SFN induces lysosomal exocytosis in a TFEB-dependent manner. (A) Confocal microscopy images showing the increased signal of LAMP1 on the PM in nonpermeabilized primary macrophage cells with SFN (15 μM, 12 h). Nuclei were counterstained with DAPI (blue). Scale bar, 10 μm. **(B)** Surface LAMP1 staining in WT and *TFEB* KO HeLa cells with SFN (15 μM, 12 h). Scale bar, 10 μm.

Figure S8. SFN promotes lysosomal biogenesis in *NPC1* KD HeLa cells. (A) LAMP1 staining of *NPC1* KD HeLa cells upon SFN (15 μM, 12 h) treatment. Nuclei were counterstained with DAPI (blue). Scale bar, 20 μm. **(B)** Quantification analysis of LAMP1 immunofluorescence shown in **A**. N=20 randomly selected cells from *n*=3 experiments. **(C)** LysoTracker staining of *NPC1* KD HeLa cells with SFN (15 μM, 12 h) treatment. Scale bar, 20 μm. **(D)** Quantification of LysoTracker intensity shown in **C**. N=20 randomly selected cells from *n*=3 experiments. For all the panels, data are presented as mean ± s.e.m.; *** $P<$ 0.001, ANOVA.

Figure S9. TFEB expression is downregulated in NPC1 cells. Western blotting analysis of

TFEB protein levels in **(A)** NPC1-patient fibroblasts and **(B)** HeLa NPC1 cells.

Figure S10. The cytotoxic effects of SFN on various cell lines. The cell viability of SFN (15 μM, 24 h)- treated HeLa NPC1, human NPC1-patient fibroblasts, and *NPC1*$^{-/-}$ MEF cells was measured by MTT assay.

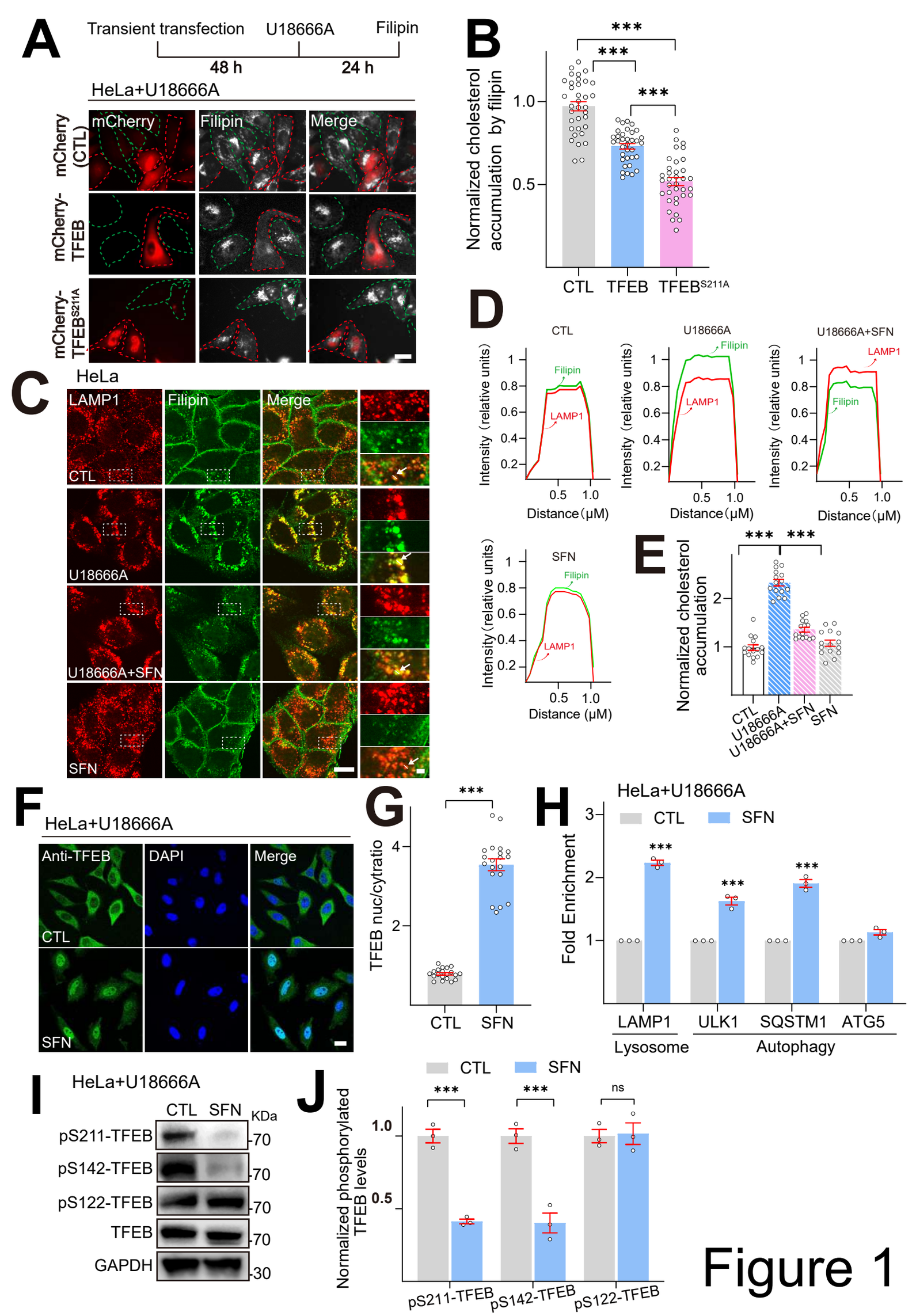
A
Transient transfection
U18666A
Filipin
48 h
24 h
HeLa+U18666A
mCherry (CTL)
mCherry-TFEB
mCherry-TFEBS211A
mCherry
Filipin
Merge
B
Normalized cholesterol accumulation by filipin
CTL
TFEB
TFEBS211A
C
HeLa
LAMP1
Filipin
Merge
CTL
U18666A
U18666A+SFN
SFN
D
CTL
U18666A
U18666A+SFN
SFN
Intensity (relative units)
Distance (μM)
LAMP1
Filipin
E
Normalized cholesterol accumulation
CTL
U18666A
U18666A+SFN
SFN
F
HeLa+U18666A
Anti-TFEB
DAPI
Merge
CTL
SFN
G
TFEB nuc/cytratio
CTL
SFN
H
HeLa+U18666A
CTL
SFN
Fold Enrichment
LAMP1
ULK1
SQSTM1
ATG5
Lysosome
Autophagy
I
HeLa+U18666A
CTL
SFN
KDa
pS211-TFEB
pS142-TFEB
pS122-TFEB
TFEB
GAPDH
70
30
J
CTL
SFN
Normalized phosphorylated TFEB levels
pS211-TFEB
pS142-TFEB
pS122-TFEB
ns
Figure 1

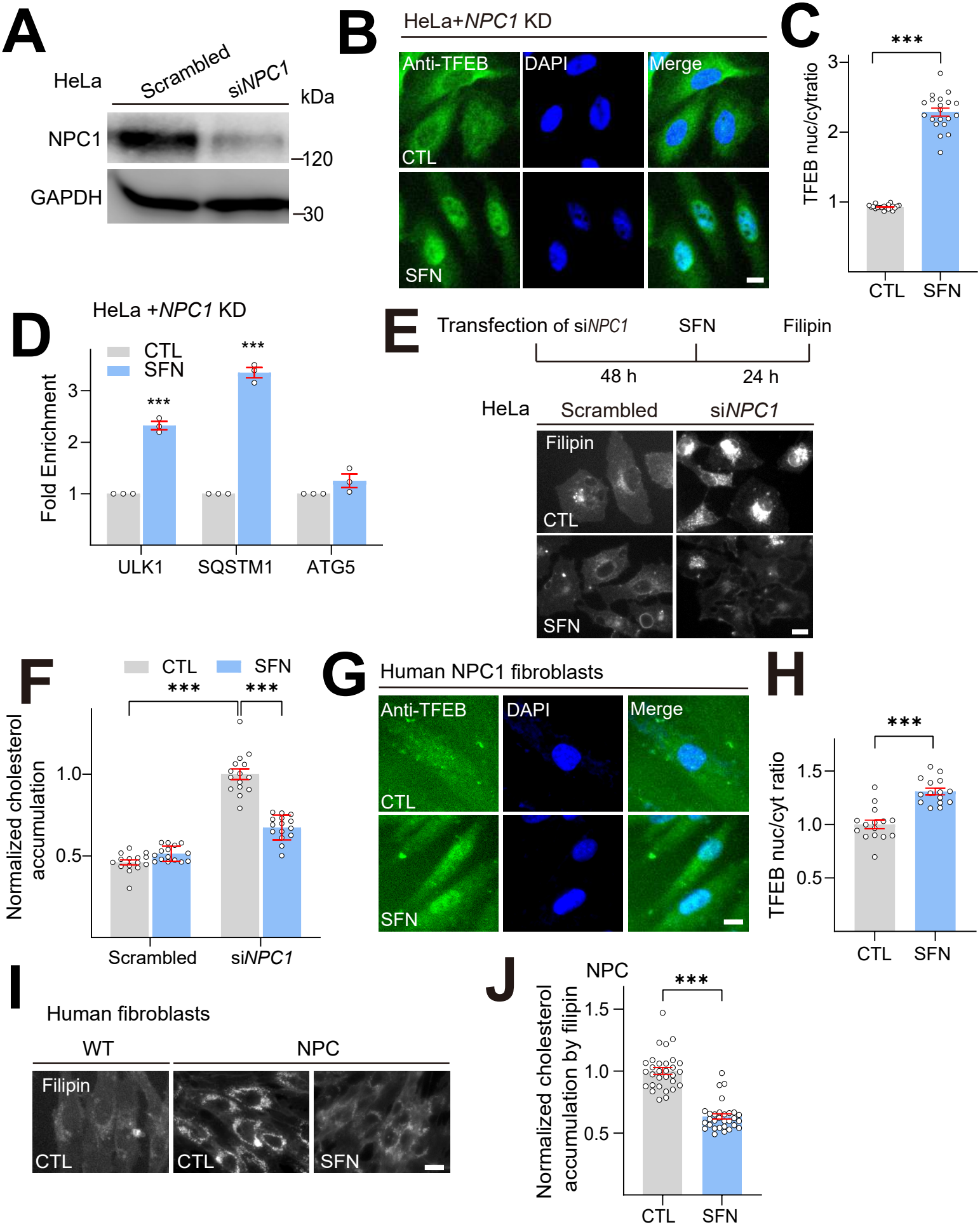
A
HeLa
Scrambled
siNPC1
kDa
NPC1
120
GAPDH
30
B
HeLa+NPC1 KD
Anti-TFEB
DAPI
Merge
CTL
SFN
C
***
TFEB nuc/cytratio
3
2
1
CTL
SFN
D
HeLa +NPC1 KD
CTL
SFN
***
***
Fold Enrichment
3
2
1
ULK1
SQSTM1
ATG5
E
Transfection of siNPC1
SFN
Filipin
48 h
24 h
HeLa
Scrambled
siNPC1
Filipin
CTL
SFN
F
CTL
SFN
***
***
Normalized cholesterol accumulation
1.0
0.5
Scrambled
siNPC1
G
Human NPC1 fibroblasts
Anti-TFEB
DAPI
Merge
CTL
SFN
H
***
TFEB nuc/cyt ratio
1.5
1.0
0.5
CTL
SFN
I
Human fibroblasts
WT
NPC
Filipin
CTL
CTL
SFN
J
NPC
***
Normalized cholesterol accumulation by filipin
1.5
1.0
0.5
CTL
SFN

Figure 2

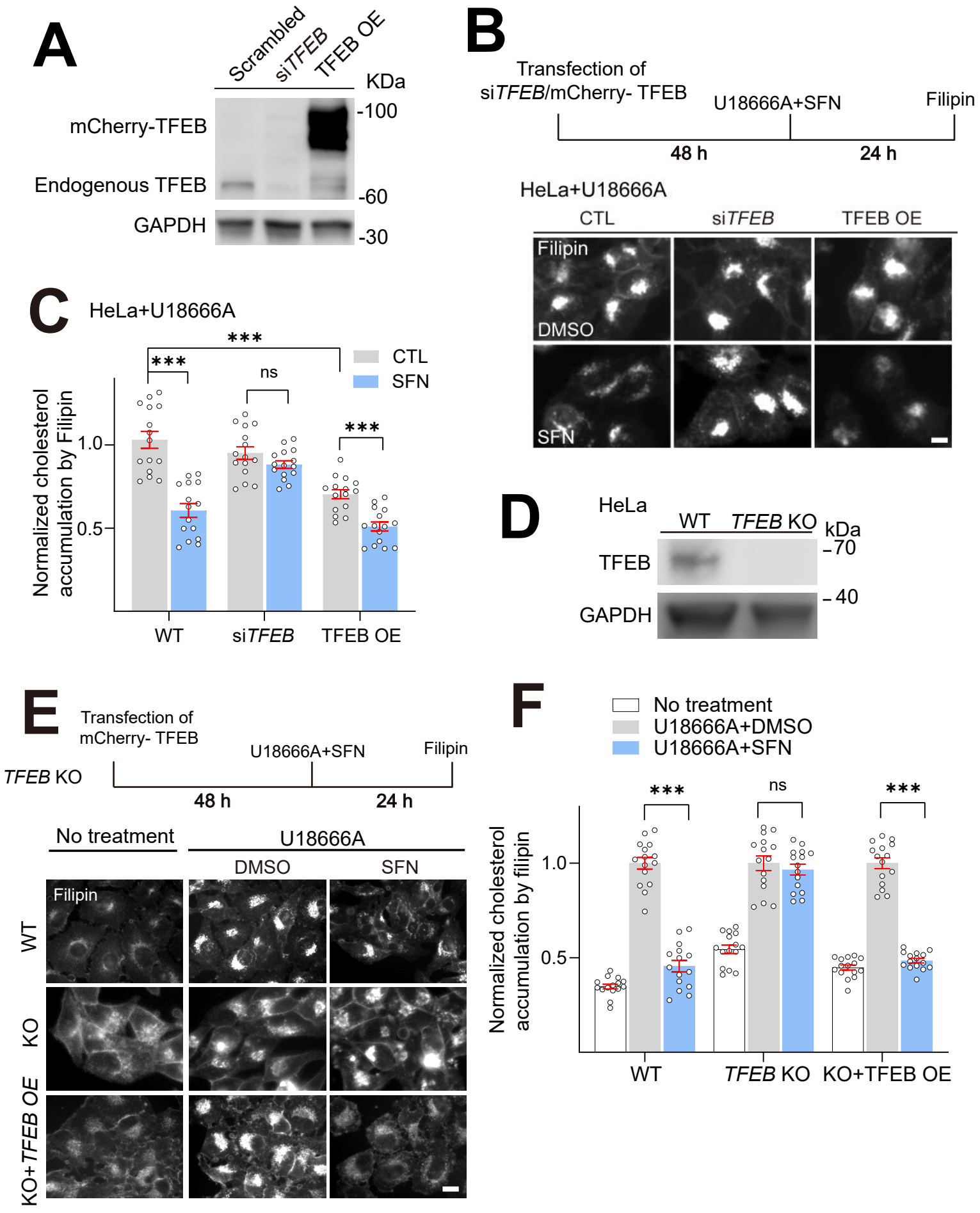
A
Scrambled
siTFEB
TFEB OE
KDa
mCherry-TFEB
Endogenous TFEB
GAPDH
-100
-60
-30
B
Transfection of
siTFEB/mCherry- TFEB
U18666A+SFN
Filipin
48 h
24 h
HeLa+U18666A
CTL
siTFEB
TFEB OE
Filipin
DMSO
SFN
C
HeLa+U18666A
CTL
SFN
Normalized cholesterol accumulation by Filipin
1.0
0.5
***
ns
WT
siTFEB
TFEB OE
D
HeLa
WT
TFEB KO
kDa
TFEB
GAPDH
70
40
E
Transfection of
mCherry- TFEB
TFEB KO
U18666A+SFN
Filipin
48 h
24 h
No treatment
U18666A
DMSO
SFN
Filipin
WT
KO
KO+TFEB OE
F
No treatment
U18666A+DMSO
U18666A+SFN
Normalized cholesterol accumulation by filipin
1.0
0.5
***
ns
WT
TFEB KO
KO+TFEB OE

Figure 3

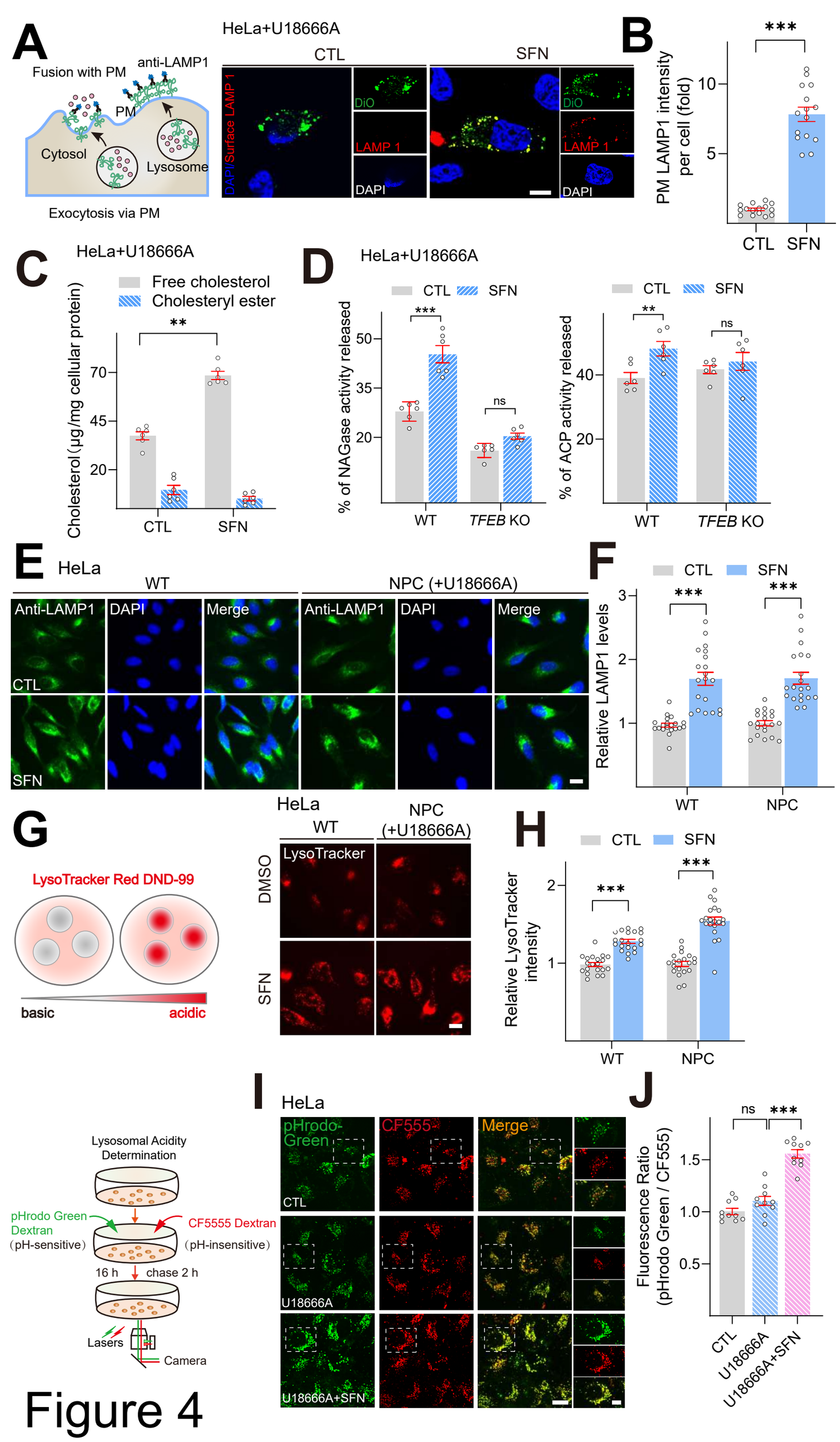
A
Fusion with PM
anti-LAMP1
PM
Cytosol
Lysosome
Exocytosis via PM
HeLa+U18666A
CTL
SFN
DAPI/Surface LAMP 1
DiO
LAMP 1
DAPI
B
PM LAMP1 intensity per cell (fold)
***
CTL
SFN
C
HeLa+U18666A
Free cholesterol
Cholesteryl ester
Cholesterol (μg/mg cellular protein)
**
CTL
SFN
D
HeLa+U18666A
CTL
SFN
% of NAGase activity released
***
ns
WT
TFEB KO
% of ACP activity released
**
ns
E
HeLa
WT
NPC (+U18666A)
Anti-LAMP1
DAPI
Merge
CTL
SFN
F
CTL
SFN
Relative LAMP1 levels
***
WT
NPC
G
LysoTracker Red DND-99
basic
acidic
HeLa
WT
NPC (+U18666A)
DMSO
SFN
LysoTracker
H
CTL
SFN
Relative LysoTracker intensity
***
WT
NPC
I
Lysosomal Acidity Determination
pHrodo Green Dextran (pH-sensitive)
CF5555 Dextran (pH-insensitive)
16 h
chase 2 h
Lasers
Camera
HeLa
pHrodo-Green
CF555
Merge
CTL
U18666A
U18666A+SFN
J
Fluorescence Ratio (pHrodo Green / CF555)
ns
***
CTL
U18666A
U18666A+SFN

Figure 4

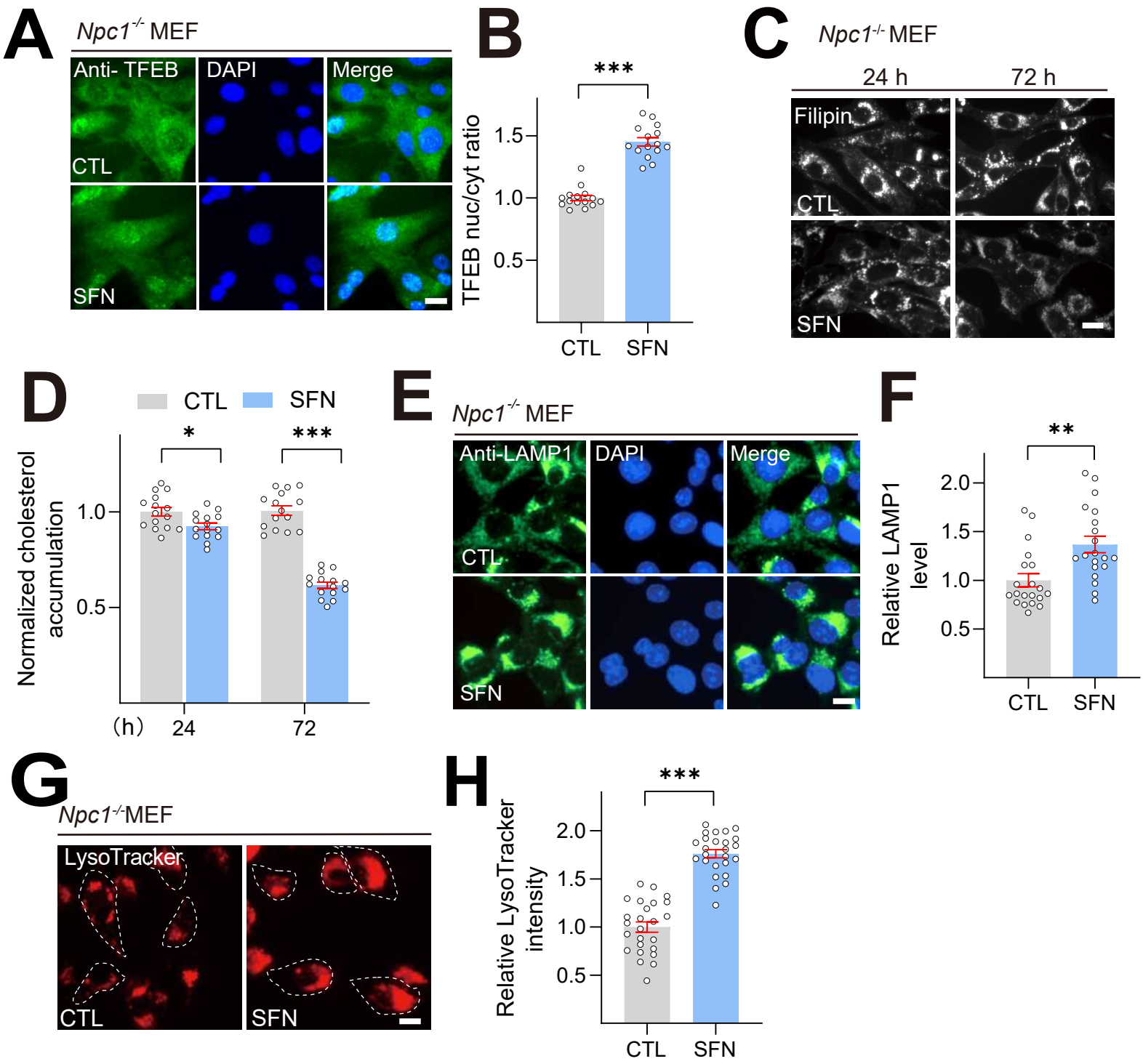
A
Npc1-/- MEF
Anti- TFEB
DAPI
Merge
CTL
SFN
B
***
TFEB nuc/cyt ratio
1.5
1.0
0.5
CTL
SFN
C
Npc1-/- MEF
24 h
72 h
Filipin
CTL
SFN
D
CTL
SFN
*
***
Normalized cholesterol accumulation
1.0
0.5
(h)
24
72
E
Npc1-/- MEF
Anti-LAMP1
DAPI
Merge
CTL
SFN
F
**
Relative LAMP1 level
2.0
1.5
1.0
0.5
CTL
SFN
G
Npc1-/-MEF
LysoTracker
CTL
SFN
H
***
Relative LysoTracker intensity
2.0
1.5
1.0
0.5
CTL
SFN

Figure 5

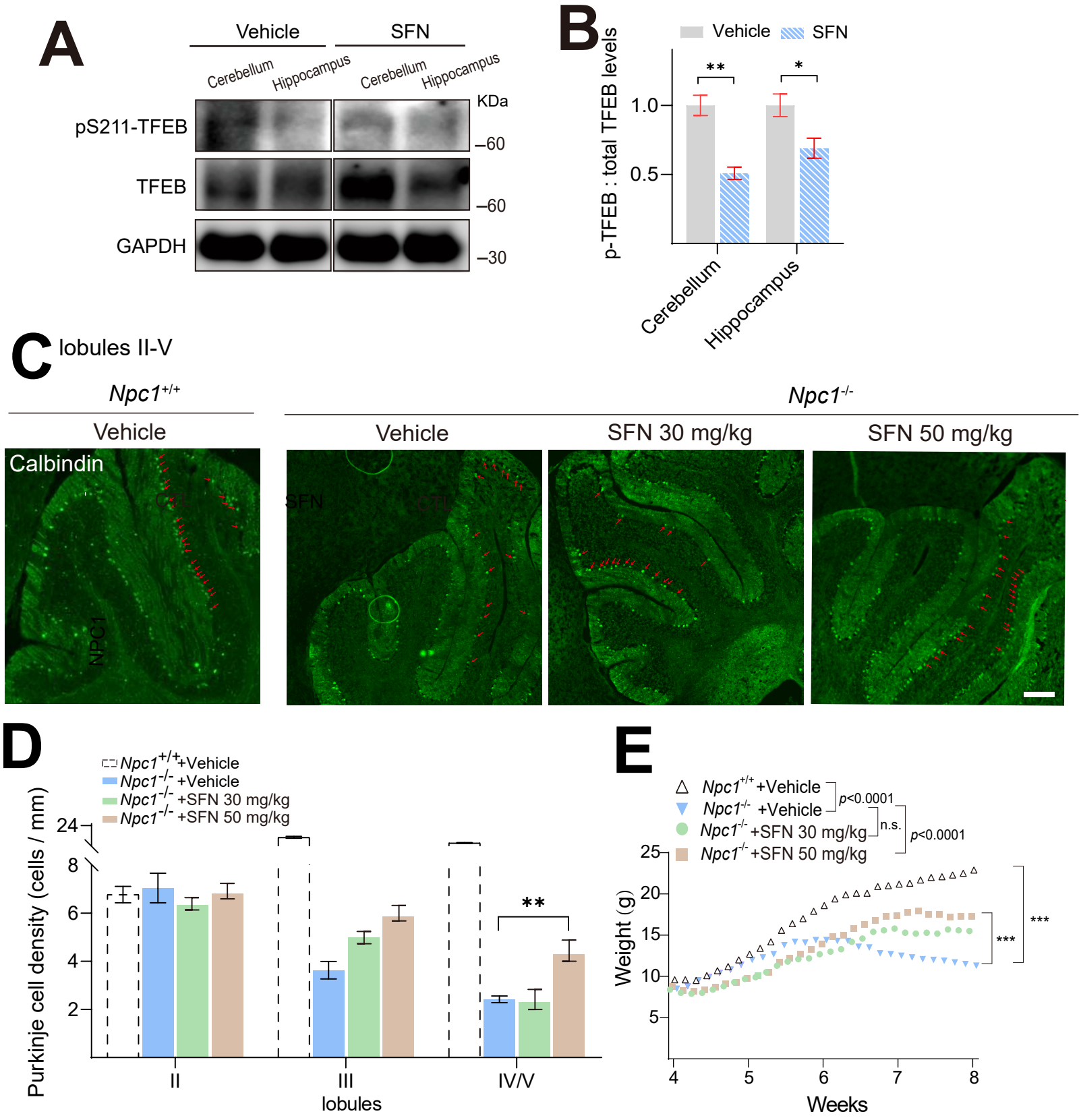
A
Vehicle
SFN
Cerebellum
Hippocampus
Cerebellum
Hippocampus
KDa
pS211-TFEB
TFEB
GAPDH
–60
–60
–30
B
Vehicle
SFN
p-TFEB : total TFEB levels
1.0
0.5
**
*
Cerebellum
Hippocampus
C
lobules II-V
Npc1+/+
Npc1-/-
Vehicle
Vehicle
SFN 30 mg/kg
SFN 50 mg/kg
Calbindin
CTL
SFN
CTL
NPC1
D
Npc1+/+ +Vehicle
Npc1-/- +Vehicle
Npc1-/- +SFN 30 mg/kg
Npc1-/- +SFN 50 mg/kg
Purkinje cell density (cells / mm)
24
8
6
4
2
**
II
III
IV/V
lobules
E
Npc1+/+ +Vehicle
Npc1-/- +Vehicle
Npc1-/- +SFN 30 mg/kg
Npc1-/- +SFN 50 mg/kg
p<0.0001
n.s.
p<0.0001
Weight (g)
25
20
15
10
5
***
***
4
5
6
7
8
Weeks

Figure 6

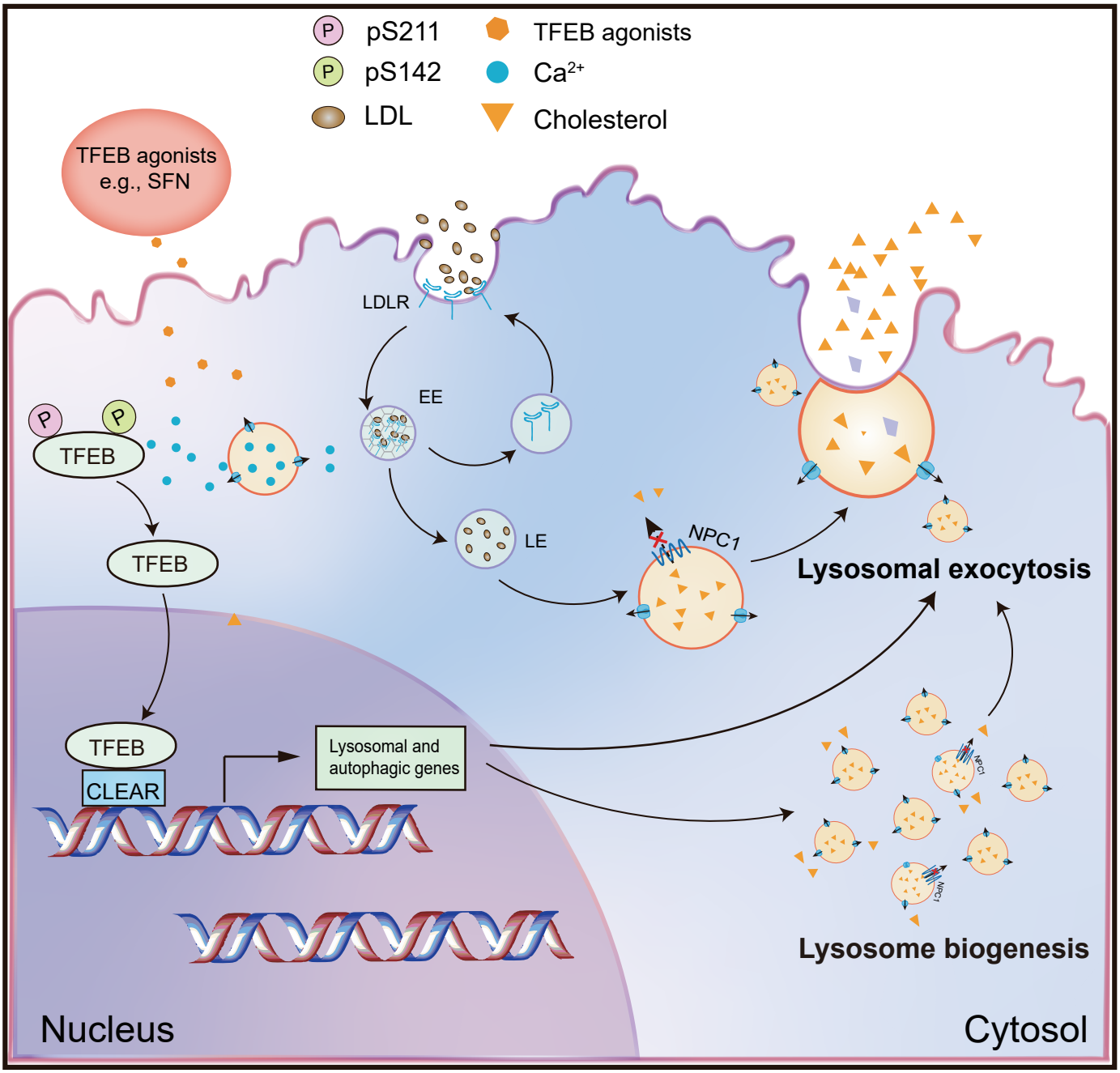
pS211
pS142
LDL
TFEB agonists
Ca2+
Cholesterol
TFEB agonists
e.g., SFN
LDLR
EE
LE
NPC1
TFEB
TFEB
TFEB
CLEAR
Lysosomal and
autophagic genes
Lysosomal exocytosis
Lysosome biogenesis
Nucleus
Cytosol

Figure 7

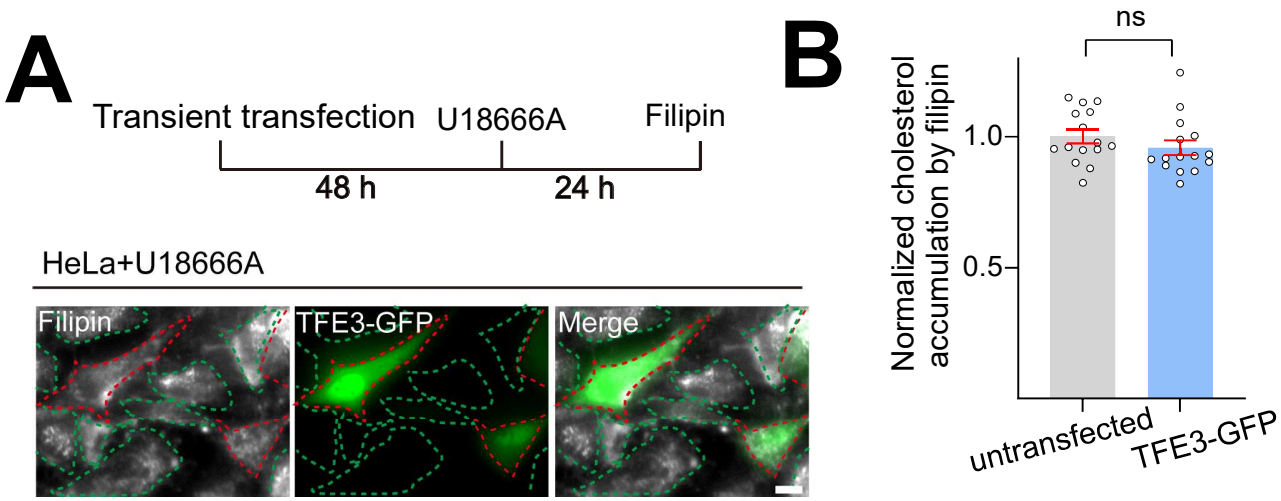

Suppl. Fig. 1

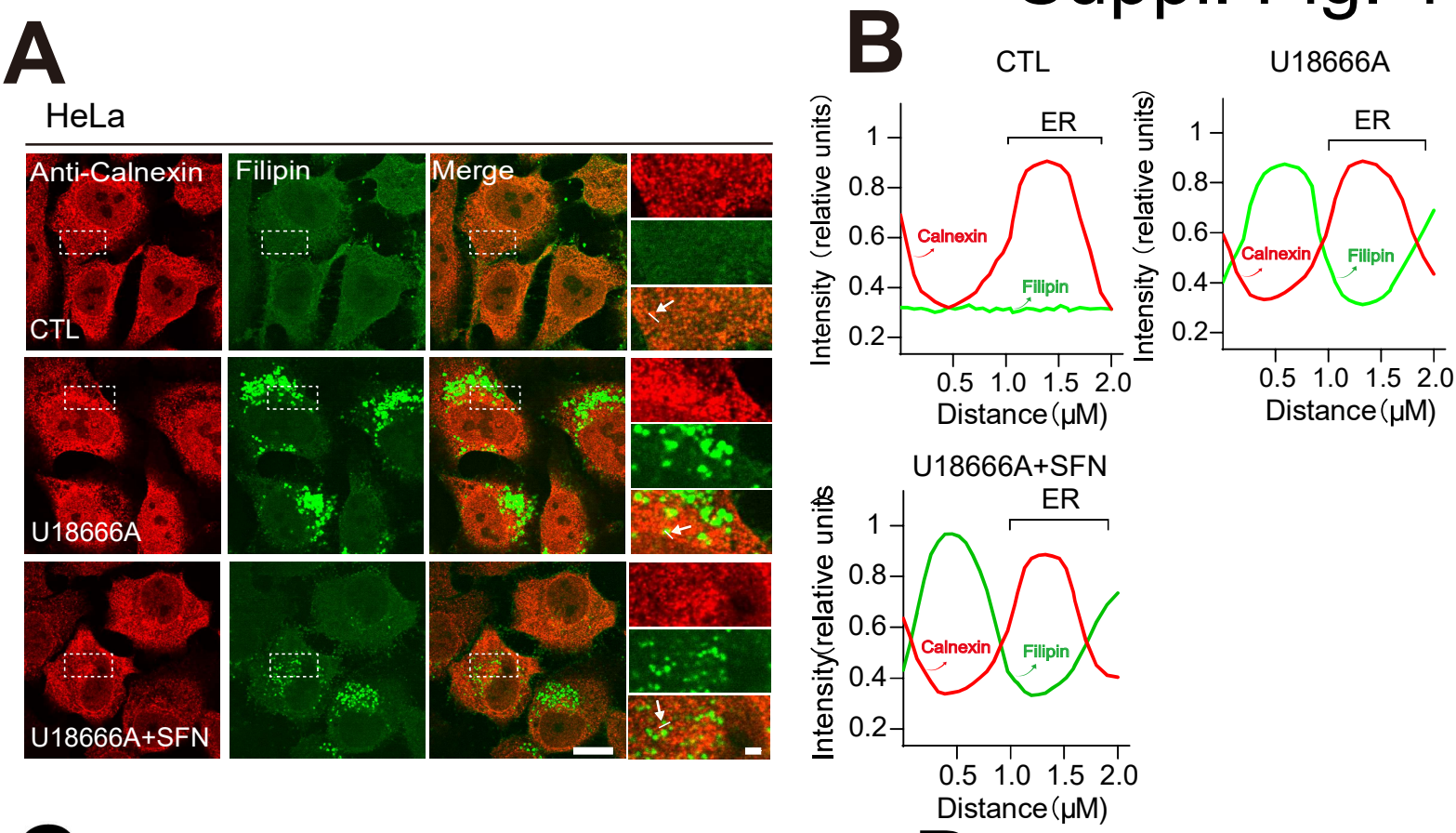

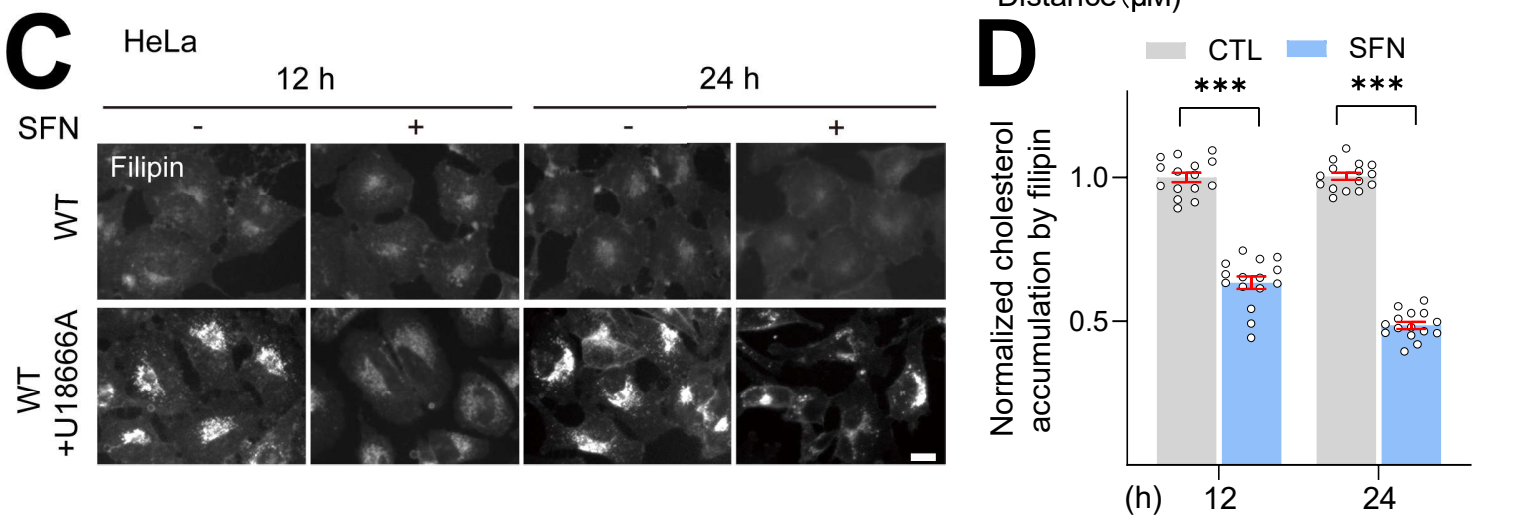

Suppl. Fig. 2

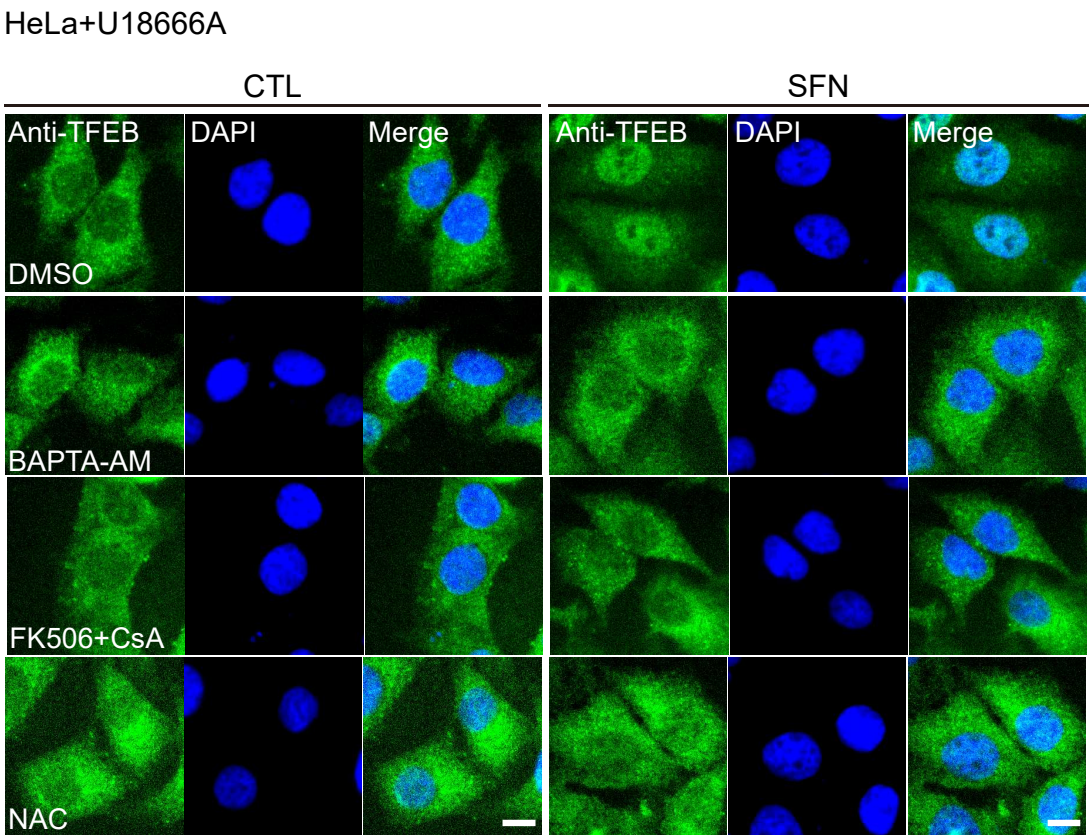

Suppl. Fig. 3

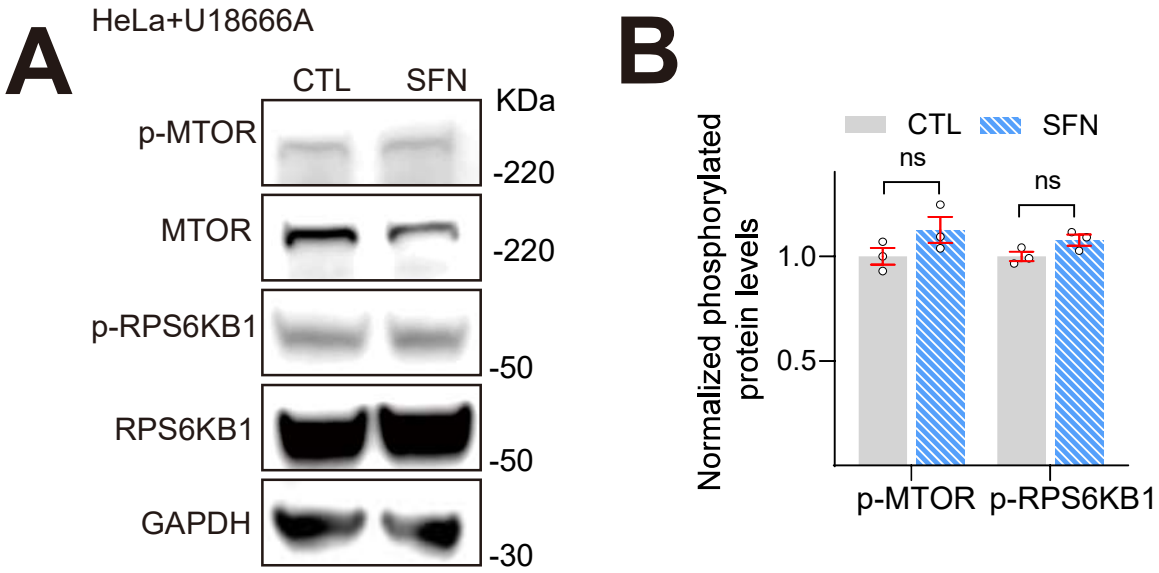

Suppl. Fig. 4

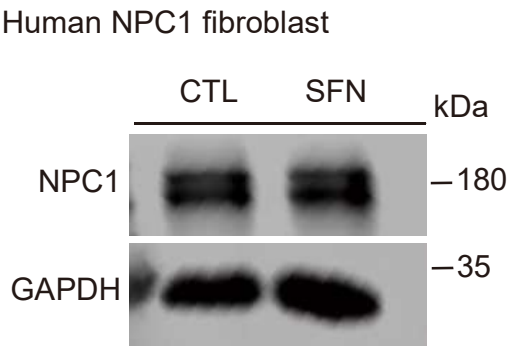

Suppl. Fig. 5

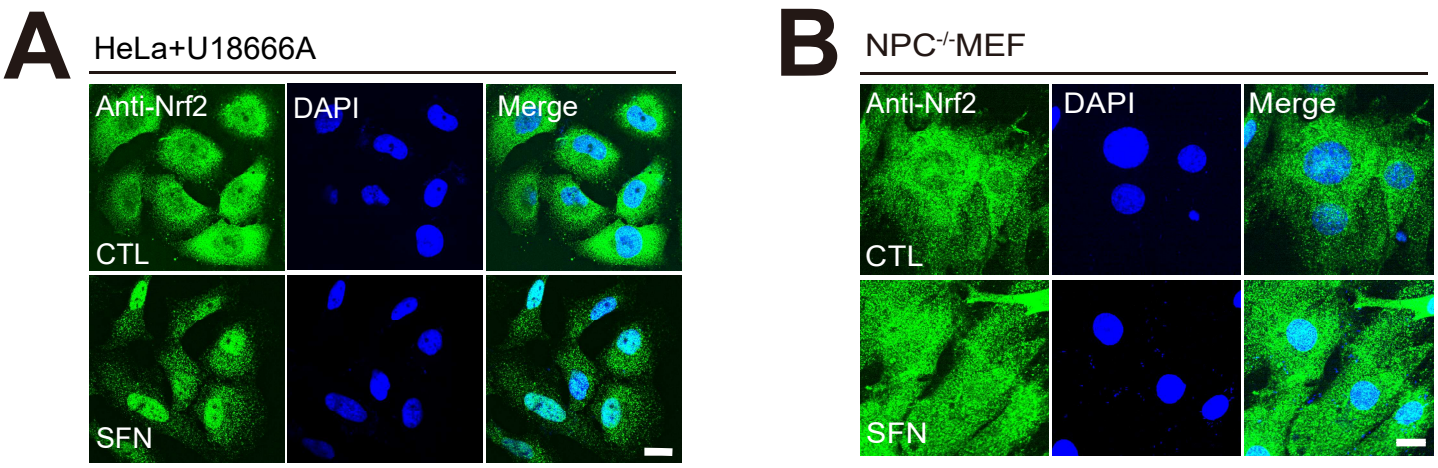

Suppl. Fig. 6

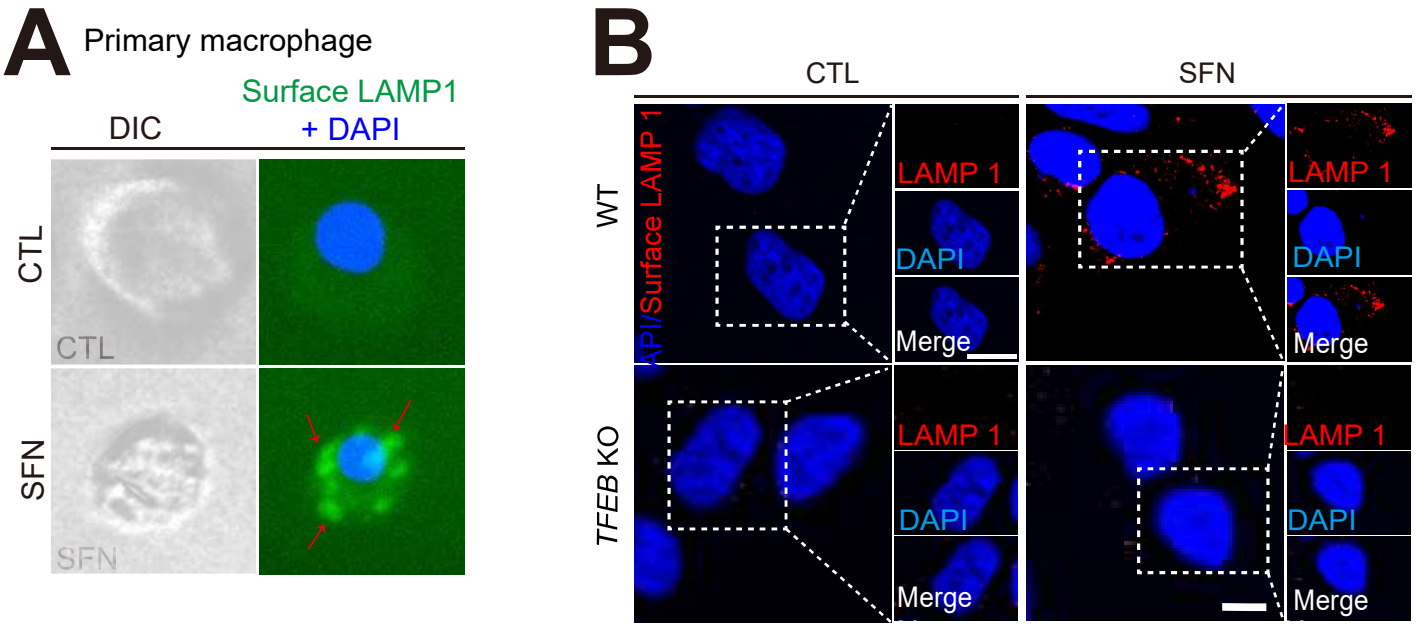

Suppl. Fig. 7

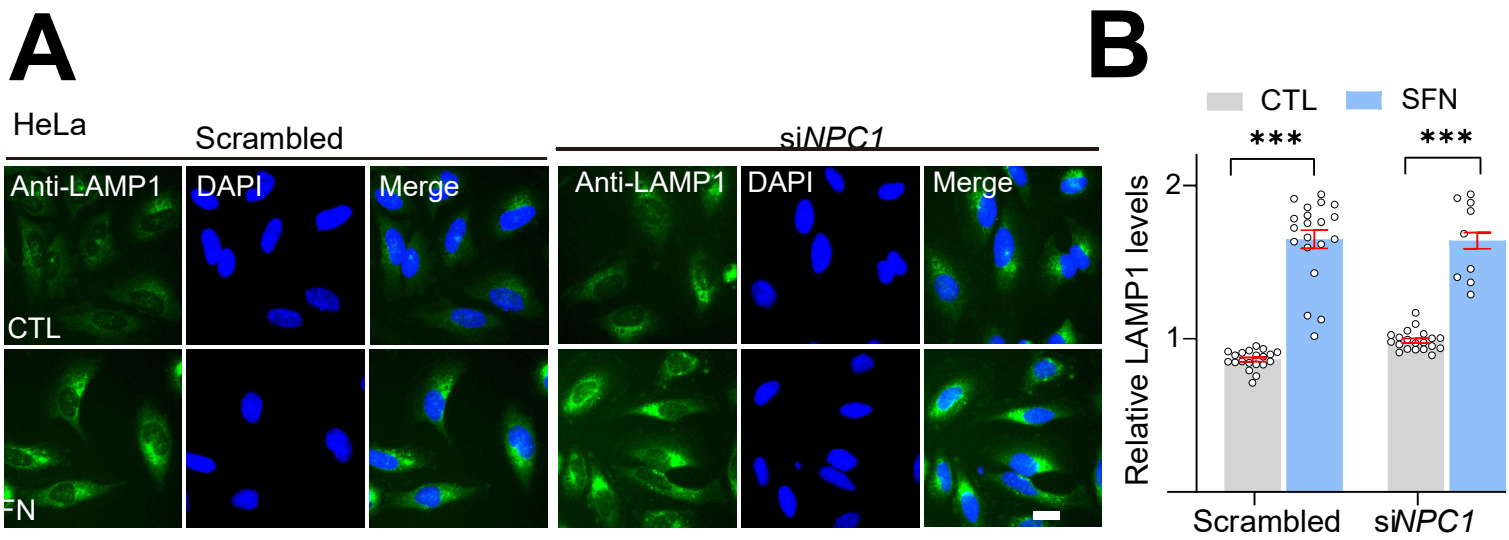

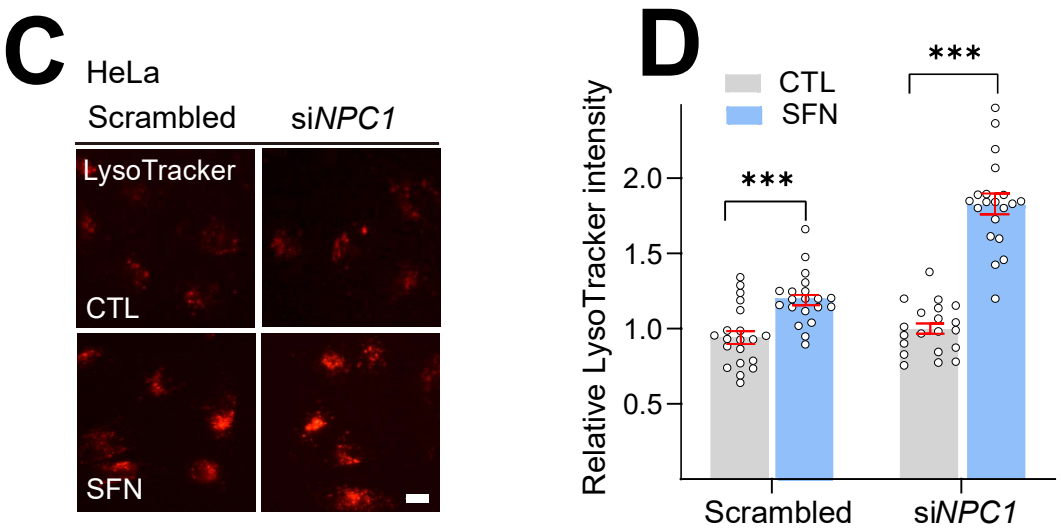

Suppl. Fig. 8

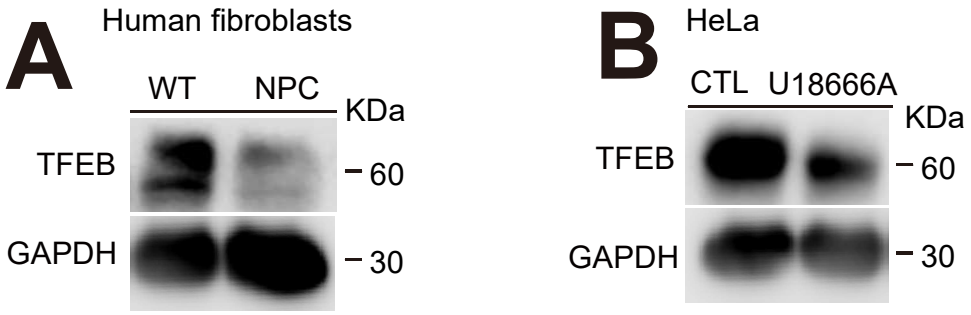

Suppl. Fig. 9

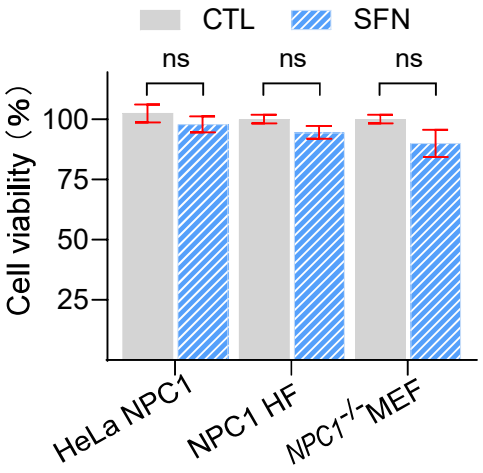
CTL
SFN
ns
ns
ns
Cell viability (%)
100
75
50
25
HeLa NPC1
NPC1 HF
NPC1-/- MEF

Suppl. Fig. 10